Investigating the Effect of Environment Shape on Bacteria Growth at the Microscale

2019 CNF REU Intern: Jacob Baker

2019 CNF REU Intern Affiliation: Biomedical Engineering, University of Arizona

CNF Project: 2019 Cornell NanoScale Science & Technology Facility Research Experiences for Undergraduates Program
CNF REU Principal Investigator(s): Guillaume Lambert, Applied and Engineering Physics, Cornell University
CNF REU Mentor(s): Matthew Henriques, Applied Physics, Cornell University
Primary Source of CNF REU Funding: National Science Foundation via the National Nanotechnology Coordinated Infrastructure (NNCI) Grant No. NNCI-1542081
Contact: jacobbaker@email.ariona.edu, lambert@cornell.edu, mdh324@cornell.edu
Website(s): https://lambertlab.io/, http://cnf.cornell.edu/education/reu/2019
Primary CNF Tools Used: ABM contact aligner, Hamatech wafer processor develop 1, P10 profilometer

Abstract:

***Escherichia coli* (*E. coli*) bacteria are sensitive to pressures exerted by their physical environment. The constraints that differently shaped growth chambers have on cell populations over time are a significant extension of this fact and play a part in characterizing bacteria growth. By utilizing the resources of the Cornell NanoScale Facility, we created a microfluidic device that features a large central fluid distribution chamber and hundreds of tiny growth chambers designed to grow bacteria at a 1 µm height display to view different test geometries and analyze their growth patterns. The device was produced by spinning micrometer thick layers of negative photoresist onto a silicon wafer and exposing to create a pattern designed in L-Edit CAD software. The wafer served as the mold for the actual device, which we then cast in PDMS. This created reproducible devices with channels for bacteria and nutrients to flow through and grow. A type of *E. coli* was genetically engineered to produce fluorescent bacteria that don't produce biofilms and were grown separately before being injected into the device. The results of this experiment play a part in widening the pool of knowledge for under what conditions bacteria thrive or stagnate, crucial data towards solving World Health Organization global health challenges such as antimicrobial resistance. Characterizing bacteria growth is one of the primary ongoing objectives of biological research. By expanding the pool of information available about how bacteria grow in different environments, application-based research on bacterial diseases, biofuels as an alternative to fossil fuels, and plasmid genetic engineering is optimized.**

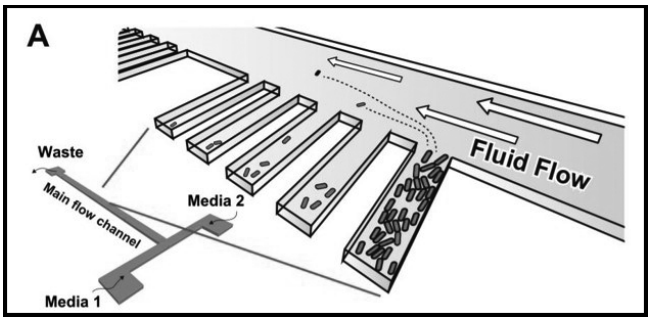

Figure 1: Microfluidic device to culture E.Coli.

Summary of Research:

We chose to focus on characterizing how *E. coli* bacteria responds to environmental conditions, specifically how the geometry containing the starting sample of bacteria limits or bolsters the growth of bacteria over time. In this preliminary qualitative research, we utilized the resources of the CNF to produce a microfluidic device, a device that would allow us to monitor bacteria growth in growth chambers one micrometer thick, while being pumped nutrients through a pneumatic system.

This microfluidic device provides a unique environment in which the bacteria and nutrients exhibit non-laminar flow, meaning that these structures can be assessed on their contribution to osmosis-based interaction with nutrients and bacteria. The microfluidic device was fabricated by developing two layers on a silicon wafer. The first layer contained a one micrometer thick etching of the entire design, notably including four growth chambers with different geometries. The first layer was purposely thin, so that the bacteria growth could be viewed efficiently, and the only effect on bacteria diffusion was the basic two dimensional geometry.

To produce this first layer, negative AZ2020 photoresist was spun onto the 4-inch silicon wafer for an even coating of resist, and then the wafer was baked at 110°C, cooled,

and then exposed to a contact aligner for 3.5 seconds for a total energy exposure of 41 mJ of energy. The wafer was then baked once more and run through the Unaxis 770 deep etch and Aura 1000 resist strip to complete the etching.

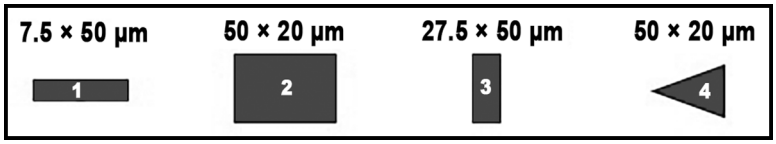

Figure 2: Geometries of four devices on the fluidic chip.

The second layer was 25 μm thick, and alternatively, we spun 2020 SU-8 photoresist on top of the wafer, which was baked at 95°C, exposed for 12 seconds for 140 mJ of energy, and then developed with SU-8 developer, completing the device. The second layer extended the height of the main flow channel.

The device itself was a long T-shape in which bacteria and nutrients could flow starting at the top of the T (Figure 1) and exited through the waste at the end of the channel. Along the main channel were a couple hundred growth chambers for each of the four geometries: a long skinny rectangle with dimensions 7.5 × 50 μm (device 1), a rectangle with dimensions 50 × 20 μm (device 2), a thick but shallow rectangle with dimensions 27.5 × 50 μm (device 3), and an isosceles triangle with dimensions 50 × 20 μm (device 4, Figure 2). Device 4 was specifically designed to study the effects of a growth chamber with smaller surface area for starter bacteria to grow than the surface area exposed to the main channel.

When hypothesizing the growth chamber geometries that would result in the highest change in cell count over time, we decided that the two largest contributing factors to the success of the designs would be the amount of surface area at the back of the device and the amount of surface area exposed to the main channel. This idea was grounded in the observation of similar microfluidic device bacteria growth experiments, where a few starter bacteria stay at the back of the device and serve as the main progenitors of new bacteria over the course of the trial period.

From the qualitative results we received in the form of pictures before the experiment began and two hours after (Figure 3, a and b), Device 1 was the only one to experience major growth, while Devices 2 and 4 had a net loss in bacteria, and Device 3 was too malformed to draw conclusions. We expected Device 4 to have poor growth due to its combination of low surface area at the back of the device and high surface area facing the main channel, but we were surprised at the lack of growth from Device 2 compared to the high growth in Device 1. We had overestimated the importance of surface area for growth at the back of the device versus the adverse effects of diffusion.

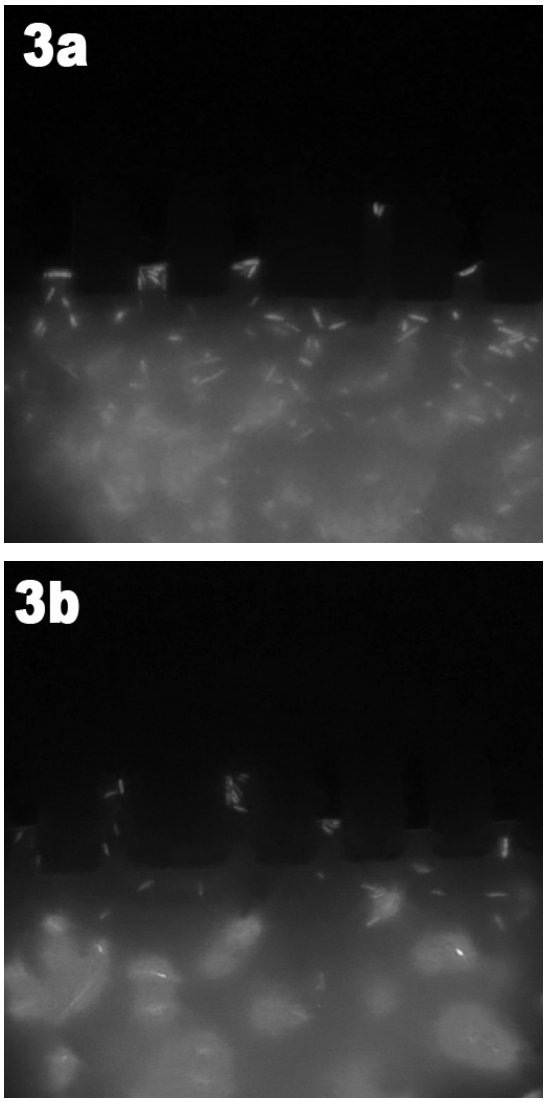

Figure 3, a and b: Fluorescent bacteria grow in Device 1 after two hours. (Find in full color on pages xiv-xv.)

Acknowledgements:

The 2019 CNF REU Program and National Science Foundation funding via the NNCI Grant No. NNCI-1542081.

References:

[1] G Lambert, E Kussell, "Quantifying Selective Pressures Driving Bacterial Evolution Using Lineage Analysis. "Physical Review X 5, 011016 (2015).

[2] G Lambert, A Bergman, Q Zhang, D Bortz, RH Austin, "Physics of biofilms: the initial stages of biofilm formation and dynamics." New J. of Physics 16 (4), 045005 (2014).

[3] "Soft Lithography: Glass/PDMS Bonding." Elveflow, www.elveflow.com/microfluidic-tutorials/soft-lithography-reviews-and-tutorials/how-to-get-the-best-process/soft-lithography-glass-pdms-bonding/.

Microfluidic Chip Manufacturing for Point-of-Care Sepsis Diagnosis

2019 CNF REU Intern: Katie Munechika

2019 CNF REU Intern Affiliation: Biomedical Engineering, University at Buffalo SUNY

CNF Project: 2019 Cornell NanoScale Science & Technology Facility Research Experiences for Undergraduates Program

CNF REU Principal Investigator(s): Dr. David Erickson, Mechanical and Aerospace Engineering, Cornell University

CNF REU Mentor(s): Taylor Oeschger, Biomedical Engineering, Cornell University

Primary Source of CNF REU Funding: National Science Foundation via the National Nanotechnology Coordinated Infrastructure (NNCI) Grant No. NNCI-1542081

Contact: km854@cornell.edu, de54@cornell.edu, tmo55@cornell.edu

Website: http://cnf.cornell.edu/education/reu/2019

Primary CNF Tools Used: ABM contact aligner, Hamatech wafer developer, UNAXIS 770 deep silicon etcher, Anatech resist strip, PDMS casting station

Abstract:

Sepsis is a life threatening condition affecting the immune system that causes the body to damage its own organs. The current diagnostic standard, consisting of monitoring organ dysfunction with a cell culture, is ineffective as it can take days, while sepsis can cause death within hours. The goal of the project is to develop a point of care microchip that can provide an accurate diagnosis from a drop of blood in 30 minutes or less by measuring the level of expression of white blood cell antigens associated with sepsis. The device utilizes a lysing and quenching process to destroy red blood cells while preserving white blood cells, and then captures white blood cells containing target antigens on antibody-coated pillars. Research has been focused on optimizing the lysing and quenching process, with a secondary goal of redesigning the pillar arrangement to maximize cell capture. In on-bench experiments, we have been able to achieve nearly 100% red blood cell lysis while maintaining less than 10% white blood cell lysis. Initial testing of cell capture on the pillars has resulted in a new design containing less pillars to increase the ease of imaging, manufacturing, and flow.

Summary of Research:

Introduction. Contributing to over 250,000 deaths per year in the US alone, sepsis alters the body's immune response to infection, leading to organ damage and immunosuppression [1]. The current diagnostic standard for sepsis includes a cell culture and a scoring system known as the Sequential Organ Failure Assessment (SOFA), which involves measuring a collection of non-specific clinical symptoms for levels of organ dysfunction [2]. This current method of diagnosis is ineffective, partly due to its lack of specificity, and because it can take days to obtain results, whereas the survival rate for sepsis decreases by 7.7% each hour that administration of antimicrobials is delayed [3]. The objective of this research is to create a microchip that can provide an accurate septic or non-septic diagnosis within 30 minutes using a drop of whole blood.

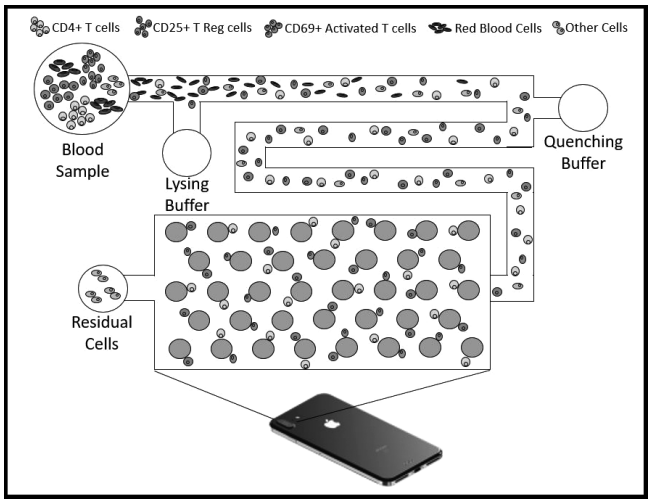

Figure 1: A simplified representation of the processing of blood and capturing of specific white blood cells on pillars in the microchip.

Design and Fabrication. The design of the microchip contains S-shaped channels and a section of antibody-coated pillars (Figure 1). When blood enters the channels, it mixes with a lysing buffer, which lyses the red blood cells allowing for easier passage of white blood cells through the device. After the blood and lysing buffer have mixed for a few seconds, a quenching buffer is added to halt the lysing process before the white blood cells are damaged. The white blood cells enter the pillar section,

and cells containing the target antigens corresponding to the pillar antibodies adhere to the pillars. The use of fluorescent antibodies allows for fluorescence smartphone imaging of the captured cells. The measured fluorescence corresponds to the level of expression of the target antigens, correlating to the presence of sepsis. To manufacture the device, first a mold is made from deep etching a silicon wafer. The mold is then cast in polydimethylsiloxane (PDMS) and plasma bonded to a glass slide. A pump system is attached via tubing to move fluid through the device.

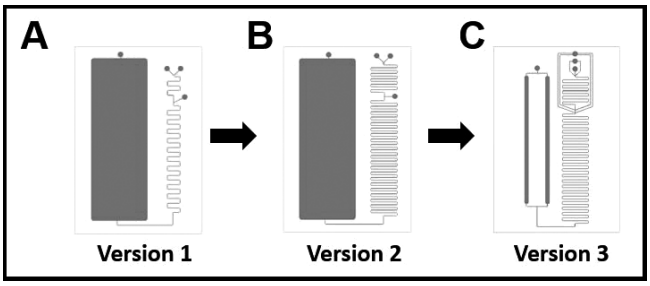

Figure 3: CAD drawings of the three versions of microchip designs.

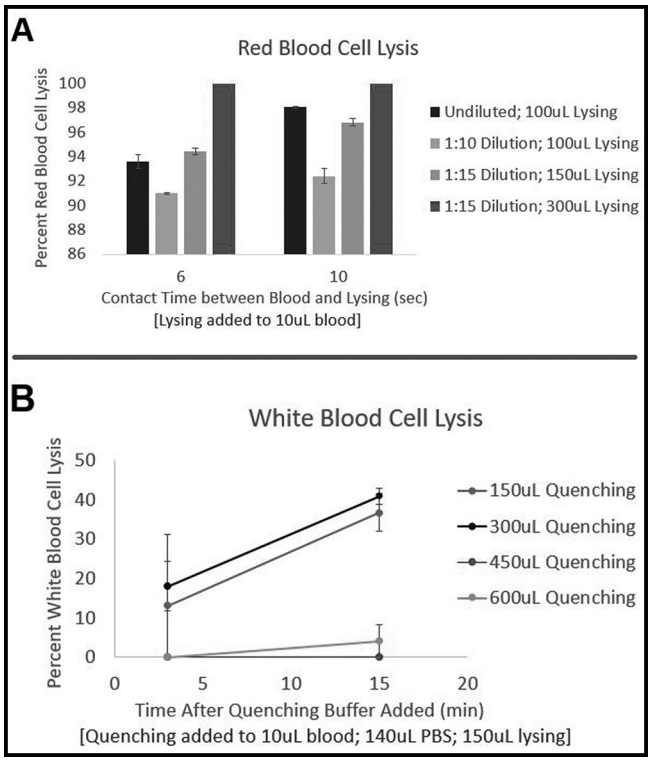

Figure 2: A) Percentage of red blood cell lysis at differing blood to lysing volume ratios for undiluted and diluted blood. B) Percentage of white blood cell lysis over time for differing quenching volumes after quenching buffer is added to diluted blood and lysing buffer.

Results and Conclusions:

A lysing buffer consisting of formic acid and saponin and a quenching buffer with sodium carbonate and phosphate buffered saline (PBS) were selected [4]. We tested various ratios of lysing buffer and quenching buffer on the bench to determine the most effective proportions to lyse the red blood cells, while limiting the damage to white blood cells. As Figure 2A shows, we were able to achieve 100% red blood cell lysis using 10 µL of blood diluted 1:15 in PBS and a lysing volume twice as large as the volume of diluted blood. We determined that the quenching volume must be at least three times that of the lysing volume to achieve less than 10% white blood cell lysis over time (Figure 2B). Based on our results, we redesigned the device with longer channels to increase contact time between the blood and buffers (Figure 3B).

The third version of the chip contains two channels and four channels extending from the lysing inlet and quenching inlet respectively to ensure that sufficient amounts of the buffers mix with the blood (Figure 3C). From a preliminary test of cell capture on the pillars, we determined that the large number of pillars was inhibiting fluid flow through the chip. Version 3 contains only 30,000 pillars, compared to the 400,000 pillars in the previous versions, and the pillar chamber is broken into two sections to allow for easier fluid flow and imaging of the device.

From an initial on-chip lysing test using Version 3, we obtained nearly 99.5% red blood cell lysis with a flow rate of 10 µL per minute, however further testing is needed to determine the accuracy of these results.

Future Work:

Further research includes testing of the on-chip lysing and quenching process using Version 3 devices, as well as optimizing and imaging the capture of CD3+ T cells, CD4+ helper T cells, CD25+ T regulatory cells, and CD69+ activated T cells on the chip. Future work also includes incorporating a low-cost, effective pumping system to replace the current 3-syringe pump system.

Acknowledgements:

Special thanks to Taylor Oeschger, Dr. David Erickson, Melanie-Claire Mallison, and the CNF staff. This work was performed in part at the CNF as part of the 2019 Cornell NanoScale Science and Technology Facility Research Experiences for Undergraduates (CNF REU) Program. The CNF is a member of the National Nanotechnology Coordinated Infrastructure (NNCI), which is supported by the National Science Foundation (Grant NNCI-1542081).

References:

[1] Rhee, et al. (2017). JAMA, 318(13), 1241.

[2] Gül, et al. (2017). TJAR, 45(3), 129-138.

[3] Kumar, et al. (2006). Crit Care Med, 34(6), 1589-1596.

[4] Hassan, et al. (2017). Nat Commun, 8(1), 15949.

Developing Microfluidic Devices for Assisted Reproductive Technologies

2019 CNF REU Intern: Darien Nguyen

2019 CNF REU Intern Affiliation: Chemistry, Winthrop University

CNF Project: 2019 Cornell NanoScale Science & Technology Facility Research Experiences for Undergraduates Program
CNF REU Principal Investigator(s): Alireza Abbaspourrad, Food Science and Technology, Cornell University
CNF REU Mentor(s): Amir Mokhtare, Food Science and Technology, Cornell University
Primary Source of CNF REU Funding: National Science Foundation via the National Nanotechnology Coordinated Infrastructure (NNCI) Grant No. NNCI-1542081
Contact: nguyend4@winthrop.edu, alireza@cornell.edu, am2964@cornell.edu
Website: http://cnf.cornell.edu/education/reu/2019
Primary CNF Tools Used: ABM contact aligner, Class II resist spinners (SU-8), plasma cleaner/PDMS casting room

Abstract:

The gaining popularity of Assisted Reproductive Technologies (ART) such as *in vitro* Fertilization (IVF) and Intracytoplasmic Sperm Injection (ICSI) calls for the introduction of more affordable and less tedious processes rather than the typical manual operations. In order for ICSI to occur, the Cumulus Oocyte Complexes (COCs) retrieved from the ovaries must be processed in order to remove the tightly-packed cumulus cells surrounding them. As of yet, this tedious and unstandardized process is being done manually by skilled embryologists, which result in variability and unavailability. The focus of this project is to develop microfluidic devices to denude the COCs for ICSI in order to reduce the tyranny of manual operations and push towards automated reproducible operations. However, many microfluidic devices are fabricated through conventional PDMS microfluidic processes that can be potentially harmful and result in loss of the precious oocytes. Herein, we report the fabrication and testing of a non-PDMS and reversibly-bonded microfluidic device using artificial eggs similar to COCs.

Summary of Research:

In order to reduce the tyranny of the current tedious, manual processes in Assisted Reproductive Technologies (ART), microfluidic devices emerge as a plausible solution. Microfluidic devices have been recently used in a few parts of the ART procedure such as sperm selection, insemination, etc. However, microfluidics has rarely been applied to improve the processing of oocytes for ICSI, which calls for the removal of the tightly-packed cumulus cells surrounding the oocyte. This research aims at developing microfluidic devices to denude cumulus cells from oocytes to not only reduce manual operations but also to increase the standardization within the ART process.

First of all, we used AutoCAD 2019 to prepare a variety of designs for the denudation of the COCs. They range from a simple single inlet/outlet port in which jagged walls intend to denude the cumulus cells off the COCs to more complex designs intending to vacuum the cumulus cells off the COCs. These designs were constructed for bovine COCs, which have a size of 400-500 μm and an oocyte size of about 150-200 μm.

We employed photolithography fabrication methods for making PDMS microfluidic devices. SU-8 molds were developed on a silicon wafer and coated with parylene to act as a mold release. PDMS was then casted on the wafer and slowly peeled from the wafer to ensure channels remain intact. The PDMS channels were then punched for the inlet and outlet ports and bonded to glass slides using a plasma oxygen bonding method.

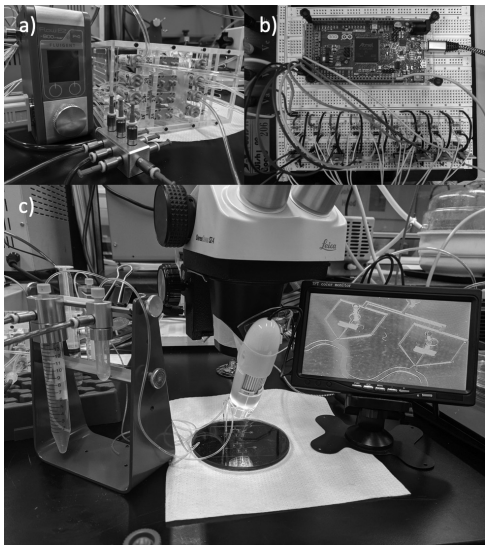

Figure 1: Equipment set-up for testing microfluidic devices. Figure 1a shows the magnetic valves and also the Fluigent pump. Figure 1b shows the Arduino microcontroller controlling the magnetic valves. Figure 1c shows the observation deck for the microfluidic devices.

In order to test these PDMS microfluidic devices, we developed an automated system consisting of a microcontroller and a set of solenoids that are connected to the computer and controlled through a graphical user interface (Figure 1). Different programs were coded for the microcontroller for each desired design. Porous, partially-crosslinked polymeric beads, dispersed in water, were used to simulate COCs and were successfully run through the channels in the PDMS microfluidic devices. However, many challenges were revealed along with this individual success.

The particles tended to stick together when traveling from the transferring tube to the microfluidic device, causing them to clog the channels. Therefore, designs were modified to a two-inlet port design where one inlet was used to only flow the media, while the other flows the particles. Although this reduced the number of clog incidents, it did not fully resolve the problem. A new microfluidic device (Figure 2) was fabricated on acrylic using the CNC Milling Machine, in order to not only prevent COCs from sticking together, but also expose them to hyaluronidase, a chemical used in oocyte processing to break down the cumulus cells.

PDMS itself is known to be deformable, allow absorption, and permit leaching, which could be harmful to cells; therefore, it potentially has a very low chance to be applied in the real and large scale. In addition, the conventional PDMS microfluidic device relies on permanent bonding to glass, which could result in damages or wasting an egg if the process were to go wrong. A new design requiring two layers of SU-8 was proposed that would apply a vacuum in order to seal the channels to a substrate that could be reversed if needed. The masks were also reverse polarized so that the channels would be etched into SU-8. The SU-8 channels were enclosed using a flat slab of PDMS and a vacuum was applied to fully enclose the channels (Figure 3).

Finally, the polymeric beads did not accurately simulate eggs due to their hydrophilic properties and the lack of an outer layer that could be removed to simulate the cumulus cells. A microfluidic device was created in order to create artificial eggs from hydrogel (Figure 4). A solid particle, acting as the oocyte, would be encapsulated in loosely-bonded hydrogel, acting as the cumulus cells.

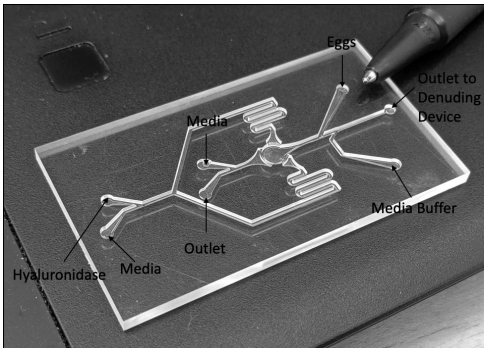

Figure 2: Acrylic microfluidic device aimed at exposing and separating the COCs.

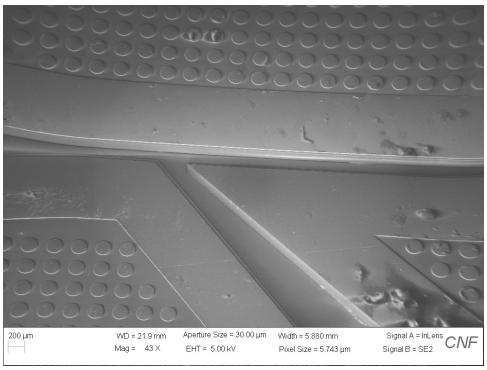

Figure 3: SEM of the SU-8 reversible vacuum design.

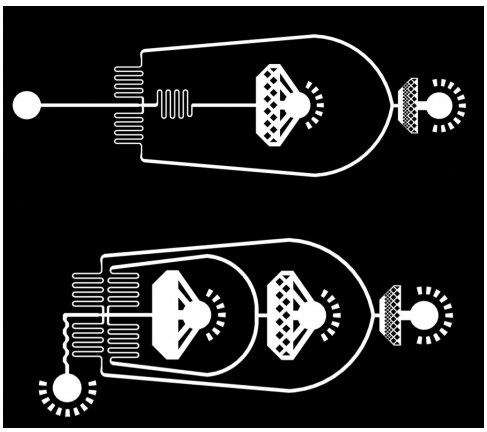

Figure 4: Mask designs for microfluidic hydrogel particle maker.

Results, Conclusion, and Future Work:

A working, reversibly-bonded, non-PDMS microfluidic device was fabricated in order to denude COCs. Artificial eggs were produced from hydrogel through another designed microfluidic device. In the future, the non-PDMS microfluidic device would be tested using actual bovine COCs to determine the effectiveness of the denudation and physical stress towards the oocyte. This would be compared to the current physical processes of denudation and be determined to be advantageous or not. In addition, further development on making the microfluidic device more automated would be in action.

Acknowledgements:

National Nanotechnology Coordinated Infrastructure, 2019 Cornell NanoScale Science and Technology Facility Research Experiences for Undergraduates (CNF REU) Program, NSF grant no. NNCI-1542081, PI: Alireza Abbaspourrad, Mentor: Amir Mokhtare, CNF REU Program Coordinator and Staff.

References:

[1] L. Weng, G. Y. Lee, J. Liu, R. Kapur, T. Toth, and M. Toner, Lab Chip, 2018, 18, 3892.

Measuring Non-Equilibrium RNA Dynamics One Molecule at a Time with SU-8 Microfluidics

CNF Project Number: 692-98

Principal Investigator(s): Lois Pollack

User (s): Alexander Plumridge

Affiliation(s): Applied and Engineering Physics, Cornell University

Primary Source(s) of Research Funding: National Institute of Health

Contact: lp26@cornell.edu, ap866@cornell.edu

Website: https://pollack.research.engineering.cornell.edu/

Primary CNF Tools Used: ABM contact aligner, class 2 resist room, VersaLaser, Heidelberg mask writer (2000)

Abstract:

Here we report the design, fabrication and implementation of an SU-8 based microfluidic mixing device to enable non-equilibrium single-molecule fluorescence measurements. The device allows rapid initiation of biological reactions, and, in a subsequent region, probing with fluorescence microscopy at times from 10ms-5s after mixing is complete. This device is used to probe the conformational dynamics of regulatory RNA molecules as they sense and bind their target and non-target ligands.

Summary of Research:

Non-equilibrium measurements are powerful tools to study biological interactions [1]. The rapid initiation of biological reactions and examination of their evolution in time, exposes information that is hidden in simple equilibrium experiments. This technique provides details on short lived intermediates, folding pathways and transition states.

Whilst the benefits of non-equilibrium measurements are numerous, such techniques are rarely applied when compared to their equilibrium counterparts. The major bottle-neck is the lack of commercially available systems to perform these experiments. Only the stopped-flow technique is widely used, but requires high sample volumes, limiting the number of kinetic measurements that have been made. Additionally, in cases where kinetic measurements are applied, the experiments report bulk averages. Therefore, sparse or short-lived intermediates are challenging to identify, and careful analysis is required to resolve the presence of intermediate states along reaction pathways [2].

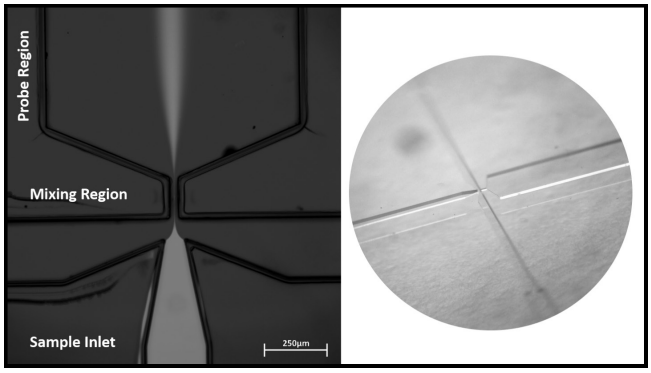

Figure 1: Two images of the SU-8 microfluidic mixing device are shown. At left, a fluorescence image is shown. Fluorescent dye (light grey), enters the sample inlet, and is compressed by flanking buffer streams through the mixing region. Here, the sample stream thins to the micron length scale, allowing rapid diffusion into the sample from the side streams. After mixing, the flow is expanded to allow probing (flow direction bottom to top). The right image shows a stereoscope image of a functional device.

Coupling microfluidic mixing to single-molecule fluorescence circumvents the above challenges. Examination of single molecules allows resolution of individual subpopulations within a sample, nanomolar concentrations are used, and ~millisecond timescales are accessible using microfluidics, with sparse sample consumption [3]. We previously designed and fabricated microfluidic mixing devices to perform such measurements (Figure 1) applying photolithography to pattern a hard material, SU-8.

In brief, a 100 μm thick layer of SU-8 2050 is spun on borofloat, after which it is baked, cured with the ABM contact aligner and developed to yield fluidic channels. A thin sealing layer of SU-8 2005 is next deposited over the top of the fluidic channels, and standard 170 μm

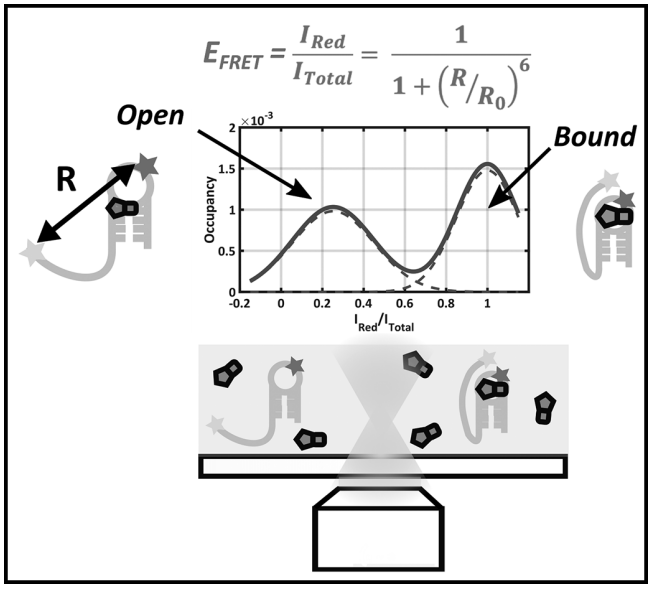

Figure 2: Single-molecule fluorescence measurements use a pair of dyes (represented as stars) to enable FRET. The relative emission of the red dye to the total emission of the dye pair is dependent on the inter-dye distance (R). When suitable positions are found for the dyes, different conformational states of RNA can be distinguished (left and right cartoons). Bound states of regulatory RNAs can be identified (in this case) by EFRET values of 1.

thick glass cover slides attached to produce a stack. The stack is baked, and the sealing SU-8 layer cured. Development removes residual SU-8 that may have entered the channels. The result is a sealed microfluidic device consisting of channel geometries defined by SU-8 sandwiched between two glass layers. The use of SU-8 significantly improves device lifetime and chemical compatibility over traditional soft polymer approaches, allowing extended experiment time with a single device.

With this device we follow regulatory ribonucleic acids (RNAs) as they bind their ligand partners. These RNA elements are labelled with two fluorescent dyes of differing colors, green and red, that form a FRET pair (Figure 2). We excite the green dye with green laser light, and measure the fluorescence emission from the red dye as a ratio of the total emission (sum of green and red dye emission), which yields the FRET efficiency value EFRET. The red emission depends on the inter-dye distance, with smaller inter-dye distances yielding EFRET values that are closer to 1. Probing single-molecules at a time, a distribution of inter-dye distances (EFRET) can be built that resolves subpopulations within our RNA sample. When bound to their ligand partners, a value close to one is expected; unbound states have larger inter-dye distances, and thus a lower EFRET value.

Pairing our microfluidic mixing device with single-molecule fluorescence measurements, we can rapidly introduce different ligand partners to our RNA sample, and watch the conformational transitions at varying times after mixing is complete. The resulting picture illustrates transitions between conformational states in the sample, and furthermore, provides quantitative measurement of rates and bound fractions for differing conditions. The results (Figure 3), show differences in the rates between two ligand partners for this particular RNA. Binding of the target (native) PreQ1 ligand occurs in ~ 500 ms, whilst the off-pathway Guanine binds in ~ 5000 ms.

The conformational re-arrangements required to transition from the unbound to the bound state are much more energetically favorable in the case of PreQ1 than for Guanine. The small differences in chemical composition of these two partners speaks to the highly evolved specificity of this RNA for its native ligand [4].

References:

[1] Al-Hashimi, H. M.; Walter, N. G. Curr. Opin. Struct. Biol. 2008, 18 (3), 321-329.

[2] Daniels, K. G.; Suo, Y.; Oas, T. G. Proc. Natl. Acad. Sci. 2015, 112 (30), 9352-9357.

[3] Wunderlich, B.; Nettels, D.; Benke, S.; Clark, J.; Weidner, S.; Hofmann, H.; Pfeil, S. H.; Schuler, B. Nat. Protoc. 2013, 8 (8).

[4] Plumridge, A.; Pollack, L. In preparation 2019.

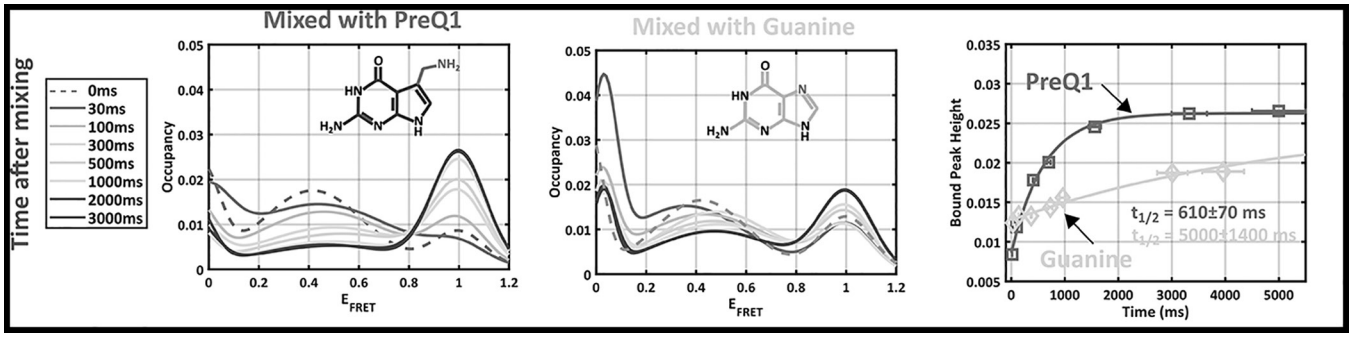

Figure 3: Pairing microfluidic mixing with single-molecule fluorescence allows us to observe RNA transitions from open to bound states at various times after mixing with ligand. In this case we probe transitions after mixing the on path (native) PreQ1, and the off path Guanine (non-native) ligands. Plotting the bound peak height as a function of time after mixing (far right) shows large differences in rates for this conformational change, despite the similar structure of these two ligands (chemical structures shown inset left panels)

Body-on-a-Chip Systems for Drug Development

CNF Project Number: 731-98

Principal Investigator(s): Michael Shuler

User(s): Danielle LaValley

Affiliation(s): Nancy E. and Peter C. Meinig School of Biomedical Engineering, Robert Frederick Smith School of Chemical and Biomolecular Engineering; Cornell University

Primary Source(s) of Research Funding: National Center for Advancing Translational Sciences, National Science Foundation, National Institutes of Health

Contact: MLS50@cornell.edu, DJL339@cornell.edu

Primary CNF Tools Used: VersaLaser cutting and engraving CO_2 laser

Abstract:

This research involved creating a pumpless, unidirectional body-on-a-chip microfluidic device for anti-cancer drug testing. The body-on-a-chip device contains individual organ chambers representing a colon tumor, liver, and bone marrow tissue connected by microfluidic channels in a relevant physiological order. The microfluidic channels were designed with specialized valves to promote fluid flow in only one direction without backflow, mimicking blood circulation in the body.

Summary of Research:

The body-on-a-chip device was fabricated out of poly(methyl methacrylate) (PMMA) and silicone layers using the VersaLaser cutting and engraving CO_2 laser. The layered design consists of a silicone layer for cell culture, a PMMA channel layer, a sealing silicone gasket, and outer PMMA housing units (Figure 1). Once assembled, the device was placed onto a rocker platform for pumpless operation, thereby allowing easier operation and eliminating the need to external tubing and pumps. This work has been submitted for publication in Lab on a Chip [1].

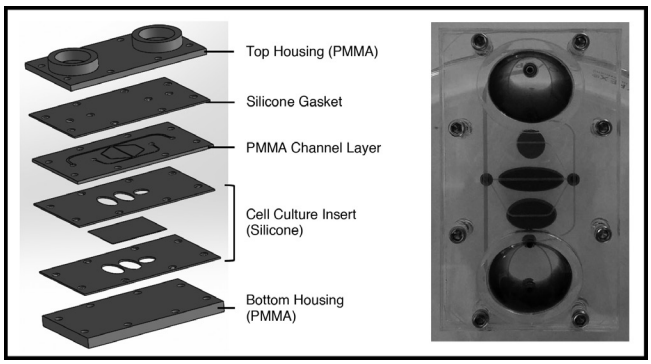

Figure 1: (Left) A schematic of the layered design for the body-on-a-chip device consisting of alternating PMMA and silicone layers. (Right) An image of the assembled device filled with blue dye to visualize the organ chambers and microfluidic channels.

References:

[1] LaValley DJ, Miller PG, Shuler ML. (2019). Pumpless, unidirectional microphysiological system for testing metabolism-dependent chemotherapeutic toxicity. Submitted to Lab on a Chip.

Body-on-a-Chip Systems for Drug Development

CNF Project Number: 731-98

Principal Investigator(s): Michael L. Shuler, Harold G. Craighead

User(s): Ying Wang, Paula Miller, Danielle LaValley

Affiliation(s): Nancy E. and Peter C. Meinig Shool of Biomedical Engineering, Robert Frederick Smith School of Chemical and Biomolecular Engineering; Cornell University

Primary Source(s) of Research Funding: National Center for Advancing Translational Sciences, National Science Foundation, National Institutes of Health

Contact: mls50@cornell.edu, hgc1@cornell.edu, ying.wang@cornell.edu, pgm6@cornell.edu, djl339@cornell.edu

Primary CNF Tools Used: VersaLaser engraver/cutter tool, ABM contact aligner, PDMS casting station, Samco UV/Ozone stripper, hot press, ObJetPro 3D printer

Abstract:

Body-on-a-chip (BOC) microphysiological systems combine biomaterials, microfluidics, microfabrication, and stem cell technologies to recreate organ structure and functionality as well as the dynamic organ-organ interactions *in vitro* [1]. They are powerful next-generation tools for human disease modeling and drug screening [2]. Here we describe two of the BOC systems that are being developed in our lab. They are fabricated with tools at CNF and designed to be used to study cancer cell extravasation and model cancer cell metastasis, and simulate immune responses.

Summary of Research:

Liver sinusoidal vascular chip for modeling colon cancer extravasation. We have designed and constructed a gravity-driven microfluidic platform for modeling the human liver sinusoidal microenvironment and investigating the extravasation of liver metastatic colorectal cancer (CRC) cells.

The device was fabricated in poly(methyl methacrylate) (PMMA). PMMA layers of desired thickness were patterned using a CO_2 laser (VersaLaser VLS3.50), and were bond together using a hot press at CNF after a 15 min UV/Ozone (Samco UV and Ozone stripper) exposure. We have also developed an apparatus to overcome the issue of sediment and aggregation of CRC cells in the feed reservoirs by introducing a propeller stirring device driven by a small stir bar on a magnetic stirrer. The propeller stirring device was designed in Inventor and fabricated using the ObJetPro 3D printer at CNF. We have tested different combinations varying in the propeller design, the positioning in the reservoir, and the stirring speed, and formulated an optimize stirring scheme that produced minimal cell sediment while preserving maximal cell viability.

We currently focus on characterizing the phenotype of liver sinusoidal endothelial cells in our microfluidic model and comparing CRC cell interactions with human liver sinusoidal endothelial cells versus human umbilical vascular endothelial cells.

Lung-on-a-Chip:

We describe a multiorgan (lung, liver and breast cancer) microphysiological system ("Body-on-a-Chip") designed to mimic both inhalation therapy and/or intravenous therapy. Microfluidic channels, chambers and medium reservoirs were etched into a layer of PMMA with the VersaLaser VLS3.5 cutting and engraving CO_2 laser (Universal Laser Systems, Scottsdale, Arizona) at the CNF. Clear silicone gaskets were also cut/etched to help seal the device and provide support for the polycarbonate membranes. This system is "pumpless" and self-contained using a rocker platform for fluid (blood surrogate) bidirectional recirculation. Our lung compartment is constructed to maintain an air-liquid interface and contained a "breathable" component that was designed to mimic breathing by simulating gas exchange, contraction and expansion of the "lung" using a reciprocating pump.

References:

[1] Wang YI, Carmona C, Hickman JJ, Shuler ML. Multiorgan Microphysiological Systems for Drug Development: Strategies, Advances, and Challenges. Adv Healthc Mater 2018;7:1701000. https://doi.org/10.1002/adhm.201701000 (2018).

[2] Sung JH, Wang YI, Narasimhan Sriram N, Jackson M, Long C, Hickman JJ, et al. Recent Advances in Body-on-a-Chip Systems. Anal Chem 2019;91:330-51. https://doi.org/10.1021/acs.analchem.8b05293 (2019).

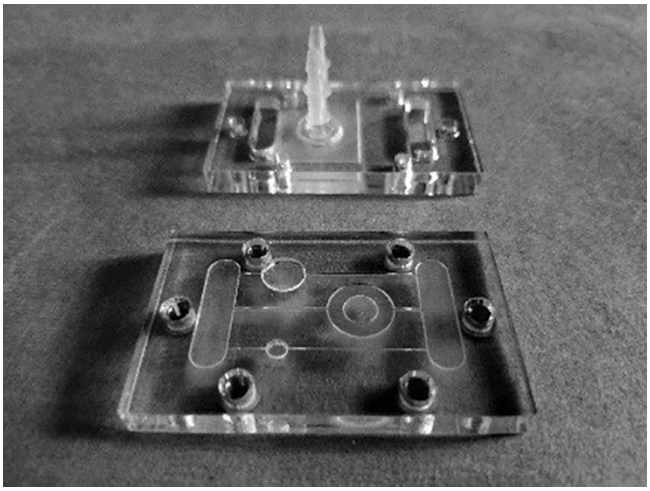

Figure 1: Actual photograph of the top and bottom frame of the microphysiological system with the breathable lung chamber.

Silicon Nitride Cantilevers for Muscle Myofibril Force Measurements

CNF Project Number: 1255-04

Principal Investigator(s): Walter Herzog

User(s): Timothy Leonard, Andrew Sawatsky

Affiliation(s): Faculty of Kinesiology, University of Calgary, Calgary, Canada

Primary Source(s) of Research Funding: Natural Sciences and Engineering Research Council of Canada, Canadian Institutes of Health Research and the Canada Research Chair for Cellular and Molecular Biomechanics

Contact: wherzog@ucalgary.ca, leonard@ucalgary.ca, ajsawats@ucalgary.ca

Website: www.ucalgary.ca/knes

Primary CNF Tools Used: GCA 5X stepper, Photolith spinners, Oxford 81 ion etcher

Abstract:

Spastic cerebral palsy (CP) is associated with increased passive muscle stress/stiffness in muscles, fascicles and fibres. However, crucial information on passive stress/stiffness on the sarcomere/myofibril level is missing. Previous research has shown that the sarcomere, the basic contractile unit of skeletal muscle, is overstretched in spastic muscle tissue compared to normal, and operates at long sarcomere lengths. At these increased lengths, the overstretched sarcomeres would have low active force-generating capacity and high passive forces, which agrees with the clinical situation whereby muscles are not only tight but also weak. Adductor longus muscle biopsies from children with CP and from typically developing children were analyzed for their *in vivo* sarcomere lengths, passive stress/stiffness, titin isoforms, and titin abundance and we found *in vivo* sarcomere lengths were increased and passive stress/stiffness and titin abundance were reduced, in CP muscle compared to controls. We conclude CP myofibrils are more compliant than control myofibrils, contrary to reports at higher structural levels. This increased compliance is caused by a reduction in the abundance of titin in CP sarcomeres. Because of the increased *in vivo* sarcomere length in CP, passive forces at functional muscle/sarcomere lengths are greater in children with CP compared to controls. Titin loss appears to be an adaptive response reducing high passive forces in CP muscles, but is insufficient to bring passive stresses to control levels, *in vivo*.

To measure muscle forces in the nano-Newton range, silicon nitride cantilever pairs were manufactured using the GCA 5x-stepper photolithography system and the Oxford 81 ion etching system at the CNF, and then used in our lab in Canada.

Summary of Research:

The aim of this research was to investigate passive properties of single CP myofibrils to see if an increase in passive stress/stiffness mirrors what has been previously reported in CP muscles, fascicles and fibres. The isolated myofibril is devoid of passive structural elements outside of the sarcomere, such as the extracellular matrix (including collagen), and so this preparation provides crucial insight into the mechanics of sarcomeres and titin in CP. The molecular spring titin is an important structural element within the sarcomere, tethering the thick filament (myosin) to the Z-discs. This protein centers the thick filament within the sarcomere and is thought to account for the majority of passive force generated when sarcomeres are stretched [1].

Methods:

Biopsies of operated adductor longus muscle were obtained and either held at the *in vivo* length for later *in vivo* sarcomere length determination, stored in a special rigor solution for generation of myofibrils, or frozen for titin analysis.

To obtain myofibrils, samples were homogenized and placed in the testing chamber [2]. The testing protocol was a ramp-hold-return design and every myofibril was lengthened (0.1 μm/sarcomere/second) from slack length (< 2.0 μm) to a sarcomere length (SL) of 2.4, 2.8, 3.2, 3.6 and 4.0 μm, sequentially. Steady-state stress and SL were measured at the end of a 1-minute hold. The cantilevers used were manufactured at the CNF and had a stiffness of 75 nN/μm.

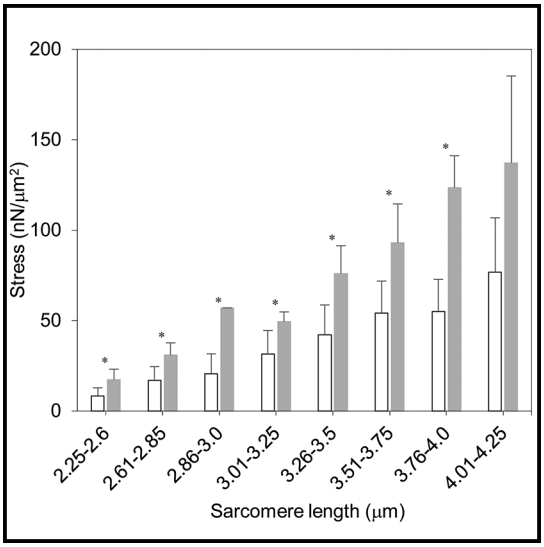

*Figure 1: Passive stress generation versus sarcomere length for CP and control adductor longus. Mean stress ± SD for CP (white) and control (grey) are significantly different at all sarcomere lengths tested, except for the longest range (> 4 μm). (*p < 0.05). The non-significant result at the longest sarcomere lengths is explained by the reduced number of observations.*

Titin isoforms were determined using 2% agarose-strengthened polyacrylamide electrophoresis gels. To assess the total titin content in the tissues, a ratio of titin to nebulin was calculated. Nebulin is a large protein found in association with the thin filament; a single nebulin molecule spanning each thin filament, thus the titin/nebulin ratio provides a measure of the abundance of titin relative to the contractile thick and thin filaments in a sarcomere.

Results:

For the CP participants, 46 adductor longus myofibrils were isolated and analyzed. For the controls, 8 myofibrils were isolated and analyzed. At all matched sarcomere length ranges (< 4 μm) passive steady-state stress was significantly lower in CP compared to control myofibrils (Figure 1). The elastic modulus for CP was 98 ± 45kPa, significantly lower than in controls (166 ± 22kPa, p = 0.0005).

Titin molecular weights for CP and control tissues were 3611 ± 41kDa and 3615 ± 8kDa, respectively (no difference: p = 0.76). The ratio of titin-nebulin content for CP was 1.47 ± 0.37 and for control was 3.26 ± 0.16 (p = 0.004). This difference is indicative of a reduced titin content relative to an unchanged nebulin content within the sarcomeres of the CP muscle. *In vivo* sarcomere lengths were much greater in CP than in typically developing children (3.6 μm versus 2.7 μm).

Discussion and Conclusions:

Passive stresses are much lower in CP myofibrils compared to typically developing control myofibrils. This finding is in contrast to results found on the single fibre, fascicle and muscle level, and as such, appears to be an adaptation to reduce an already excessive passive force in spastic muscles. Despite the much lower stresses in CP compared to control myofibrils at matched sarcomere lengths, passive stresses at *in vivo* sarcomere lengths are much greater in CP than in typically developing children because the CP sarcomeres are over-stretched (3.6 μm versus 2.7 μm). A loss in titin content in CP muscle was found to be associated with decreases in the passive peak stress and elastic modulus of CP sarcomeres, which may be an adaptive response resulting in a more compliant myofibril, to partially offset the high passive stresses experienced at long *in vivo* sarcomere lengths of CP patients [3].

References:

[1] Bartoo, M. L., Linke, W. A., and Pollack, G. H. Basis of passive tension and stiffness in isolated rabbit myofibrils. Am. J. Physiol. 273, C266-276 (1997).

[2] Joumaa, V., Rassier, D.E., Leonard, T.R., Herzog, W. The origin of passive force enhancement in skeletal muscle. Am. J. Physiol. Cell Physiol. 294, C74-78. https://doi.org/10.1152/ajpcell.00218.2007 (2008).

[3] Smith, L. R., Lee, K. S., Ward, S. R., Chambers, H. G., and Lieber, R. L. Hamstring contractures in children with spastic cerebral palsy result from a stiffer extracellular matrix and increased *in vivo* sarcomere length. J. Physiol. 589, 2625-2639 (2011).

Unzipping an Array of DNA Molecules by Resonator Based Nanophotonic Tweezers

CNF Project Number: 1738-08

Principal Investigator(s): Michelle D. Wang

User(s): Fan Ye

Affiliation(s): a) Department of Physics, Cornell University; b) Howard Hughes Medical Institute

Primary Source(s) of Research Funding: Howard Hughes Medical Institute

Contact: mdw17@cornell.edu, fy72@cornell.edu

Website: http://wanglab.lassp.cornell.edu/

Primary CNF Tools Used: ASML deep ultraviolet stepper, Oxford 100 plasma etcher, Unaxis 770 deep Si etcher, Heidelberg mask writer DWL2000, SÜSS MA6-BA6 contact aligner, Gamma automatic coat-develop tool, LPCVD Nitride - B4 furnace, Wet/Dry Oxide - B2 furnace, AJA sputter deposition, CVC sputter deposition, GSI PECVD, Oxford PECVD, SC4500 odd-hour evaporator, Zeiss Supra and Ultra SEMs

Abstract:

Optical trapping has become a major technique widely used in biological and materials sciences, on size scales ranging from the single molecule to the cellular level, and force scales ranging from sub piconewton (pN) to tens of pN [1]. The rapid development of nanofabrication techniques in the past few decades has bolstered the emergence of nanophotonic evanescent-field traps. The ability of nanostructures to direct and confine light beyond the diffraction limit enables miniaturized, on-chip devices with abilities beyond traditional microscope-based optical tweezers [2]. The Wang lab has developed and implemented such an on-chip device based on Si or Si_3N_4 waveguides, coined a nanophotonic standing-wave array trap (nSWAT), that allows for controlled and precise manipulation of trapped single biomolecule (such as DNA) arrays via microparticle handles [3-6]. We present here the latest development of the nSWAT platform based on a resonator design that achieves large enough manipulation forces for unzipping an array of DNA molecules. This benchmark achievement is one step closer to the full realization of nanophotonic tweezers' capabilities, promising increased accessibility and expansion of these platforms to a wide range of biological and biomedical research topics.

Summary of Research:

Over the past decade, the Wang lab has demonstrated a high-throughput, near-field nanophotonic trapping platform that achieves stable trapping and precision manipulation of microparticles [3-6]. The kernel of this platform is the formation of standing waves along a nanophotonic waveguide: by counter propagating two coherent laser beams along a single-mode nanophotonic waveguide. The antinodes of the standing wave form an array of stable optical traps. We call this type of trap a nanophotonic standing-wave array trap (nSWAT). By tuning the phase difference between the two counter-propagating laser beams via thermo-optic effect, the antinode locations can be precisely repositioned, and consequently, the optical trap positions can be precisely manipulated. The nSWAT platform holds the capability for high throughput precision measurements for single biomolecules.

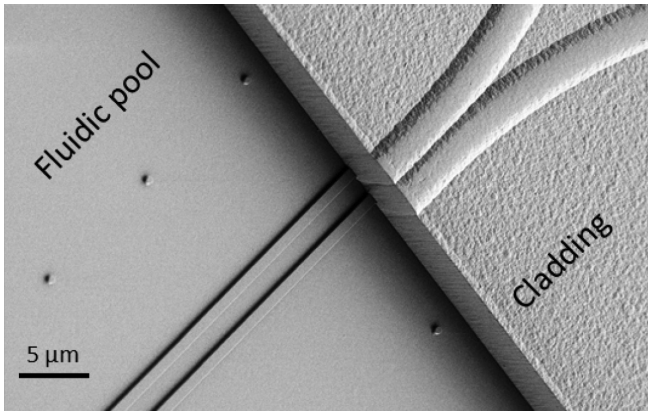

Figure 1: A tilted-angle SEM image of the step boundary of the fluid pool region. Inside the fluid pool region, the two parallel Si_3N_4 waveguides trap two arrays of polystyrene microbeads (380 nm diameter) with DNA molecules tethered in between. The dot arrays near the parallel waveguides are fiducial markers for local position tracking.

In 2018, we have implemented a major upgrade of the nSWAT platform, including the following three aspects: (1) We have implemented a resonator based design for ultimate local intensity enhancement into the nSWAT devcies. Compared to previous designs, this resonator design gives the highest force enhancement factor, limited only by the total scattering loss of the trapped beads onto the waveguide. We have measured around three times force enhancement, larger than our previous force-double design [5]. (2) We have implemented a balanced layout and differential operation mode for the micro heaters. This greatly reduced the response time of the micro heaters (from ~ 30 μs to ~ 1 μs). This is shown to be crucial for maintaining high trapping forces for a trapped bead under strong biased forces under single molecule manipulations. (3) We have also designed a special sample holder for the nSWAT chip that can greatly reduce (by two orders of magnitude) the thermal drift of the sample caused by the micro heaters. This greatly enhanced the thermal stability of the nSWAT devices. Thanks to the above described improvements, we have achieved DNA unzipping on the nSWAT devices for the first time

In the past year, we have continued optimizing the nSWAT platform to achieve our final goal of unzipping an array of DNA molecules. We have further optimized the flow chamber design of the nSWAT devices to achieve better DNA molecule trapping efficiency. We have also implemented SU-8 layer as the anti-corrosion protection layer for the nSWAT device that works significantly better than the Si_3N_4 protection layer we used before [4]. With all these improvements, we are looking forward to the achievement of trapping and unzipping an array of DNA molecules in the near future.

Our development and improvement of the nSWAT platform has led to five publications in the past few years [2-6], and more to come later this year.

References:

[1] J. L. Killian, F. Ye, M. D. Wang, "Optical Tweezers: A Force to Be Reckoned With" Cell 175 (6), 1445-1448 (2018).

[2] J. E. Baker, R. P. Badman, and M. D. Wang, "Nanophotonic trapping: precise manipulation and measurement of biomolecular arrays" WIREs Nanomed Nanobiotechnol. e1477 (2017).

[3] M. Soltani, J. Lin, R. A. Forties, J. T. Inman, S. N. Saraf, R. M. Fulbright, M. Lipson, and M. D. Wang, "Nanophotonic trapping for precise manipulation of biomolecular arrays" Nature Nanotechnology 9(6), 448-452 (2014).

[4] F. Ye, R. P. Badman, J. T. Inman, M. Soltani, J. L. Killian, and M. D. Wang, "Biocompatible and high stiffness nanophotonic trap array for precise and versatile manipulation" Nano Letters 16(10), 6661-6667 (2016).

[5] F. Ye, M. Soltani, J. T. Inman, and M. D. Wang, "Tunable nanophotonic array traps with enhanced force and stability" Optics Express 25 (7) 7907-7918 (2017).

[6] R. Badman, F. Ye, W. Caravan, and M. D. Wang, "High Trap Stiffness Microcylinders for Nanophotonic Trapping" ACS Appl. Mater. Interfaces (2019) https://doi.org/10.1021/acsami.9b10041 (published online).

Development of a Salivary Microfluidic Diagnostic Device using Hot Embossing

CNF Project Number: 1872-10

Principal Investigator(s): David Erickson

User(s): Elizabeth Rey

Affiliation(s): Sibley School of Mechanical and Aerospace Engineering, Cornell University

Primary Source(s) of Research Funding: National Science Foundation

Contact: de54@cornell.edu, egr42@cornell.edu

Primary CNF Tools Used: Hot press, photolithography room, ABM contact aligner, Unaxis 770 deep Si etcher, Microdrill, Objet30 3D Printer

Abstract:

Point of care diagnostic devices allow people to get fast, accurate information about their health and well-being without the need to go to a clinic or hospital. The device that we are designing will determine the concentration of cortisol from a sample of the user's saliva. Cortisol is a steroid hormone associated with stress levels and expressed in human saliva [1,2]. This microfluidic device contains a microbead-based immunoassay that we are optimizing to determine the cortisol content from a saliva sample. The device is manufactured using a hot embossing process, which uses a silicon master made with traditional lithographic processes. The device is made from a thermoplastic called Zeonor 1020R, which is a transparent, semi-rigid plastic that can be used in large-scale manufacturing processes such as injection molding and hot embossing. Nearly all the fabrication of the device is being done in the Cornell NanoScale Facility.

Summary of Research:

The microfluidic device is made using a hot embossing process, which involves the high-temperature pressing of a mold into a piece of thermoplastic. The mold that we use in our process is made of silicon and is fabricated using photolithographic processes. The design for the mold is made using L-Edit and transferred to a photomask using the Heidelberg mask writer (DWL2000). This mask is then used to transfer a pattern to a photoresist on a silicon wafer. The photoresist (SPR-220-7.0) is spun onto a bare silicon wafer, which has been previously primed in the YES vapor prime oven, to a thickness of approximately 7 µm. After spinning, the photoresist is soft baked on a 115°C hot plate for 2 minutes and 30 seconds. The wafer is allowed to sit for an hour and then exposed using the mask and the ABM contact aligner. The wafer is again allowed to sit for an hour and then is developed using the Hamatech Steag wafer processor. The pattern is now developed and can be used to etch the silicon wafer.

We etched the wafer using the Unaxis 770 deep Si etcher to a depth of 50 µm. We monitored the etch depth and etch rate using the P10 profilometer. Upon reaching the desired depth, we removed the photoresist in the chemical strip bath. We then used the Unaxis 770 again to deposit a thin layer of fluoropolymer onto the wafer in order to prevent sticking in the hot emboss process. Our masters were then ready to be used in the hot emboss process.

The hot emboss process uses the CRC Prepreg Mini Test Press, which applies heat and even pressure. The silicon master is adhered to a glass backing, for strength, and then the plastic piece is placed on top of the master, with another glass piece on top of that. This whole stack is placed in the hot press once the hot press reaches the desired temperature and pressed for several minutes. The setup is allowed to cool below the glass transition temperature of the plastic and then the pressure is released and the plastic is de-embossed. The pattern is transferred from the master to the plastic. We then drill through-holes in a blank piece of plastic using the custom-made micro drill. In our own lab, we perform a photografting procedure to increase hydrophilicity of the Zeonor surfaces and improve bonding. This blank piece is then thermally bonded to the patterned piece to create the microfluidic device in the hot press. Our microfluidic device is now complete and ready to be turned into an immunoassay. An example can be seen in Figure 1(a).

We can now flow differently sized beads into the device to create areas for antibody-antigen-fluorophore interaction. The channels after the beads are successfully

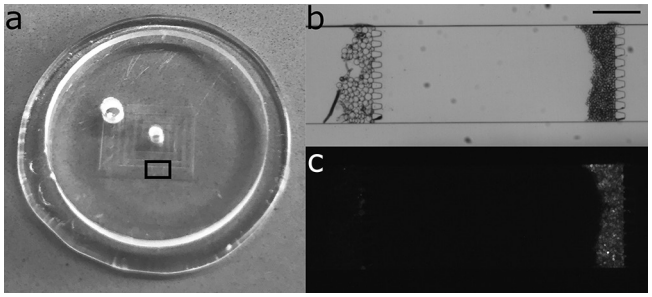

Figure 1: Microfluidic chip. a) Completed microfluidic chip with inlet at center and outlet on the left. Box depicts pillar/bead zone. b) Microscope image of channels, pillars, and different sized bead zones c) Microscope image of fluorescence on beads after flowing of AlexaFluor488 through chip.

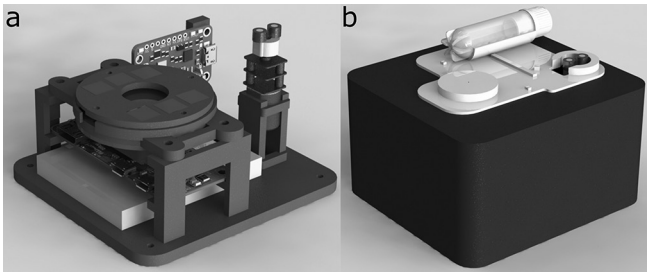

Figure 2: Rendering of 3D-printed imaging and pumping device. a) Interior assembly including Raspberry Pi Zero W, optical components, geared motor, custom peristaltic pump head, lithium-ion battery, and Powerboost 1000C. b) Exterior of device with disposable cassette attached via snap fit.

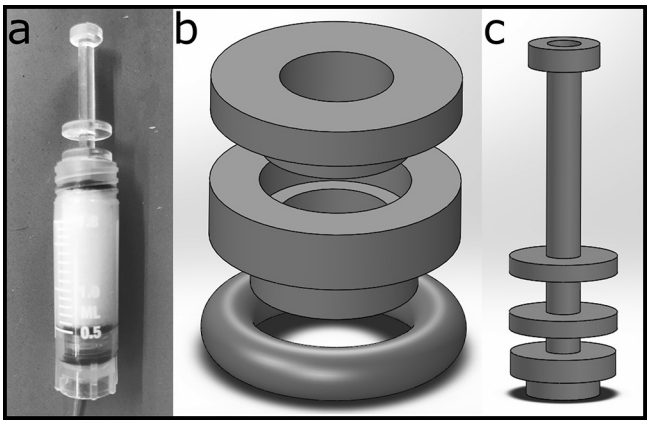

Figure 3: Saliva filtration setup. a.) Image of complete filtration setup. b.) Custom filter holder with two pieces that hold a circular filter between them and an O-ring beneath. c.) Plunger to compress saliva swab and push saliva through filter.

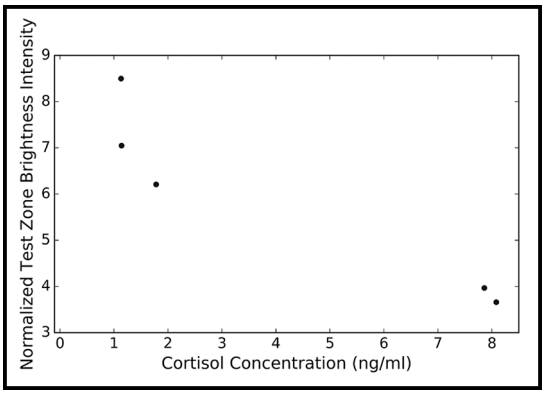

Figure 4: Preliminary fresh filtered saliva results. n=1.

added can be seen in Figure 1(b). The differently-spaced pillars allow two zones with beads with different antibodies to be separated by size. We then flow fluid with cortisol and AlexaFluor488-labeled antibodies through the device using a custom microfluidic peristaltic pump and measure the brightness of the fluorescence at the bead zones with a microscope or with our portable imaging and pumping device. A microscope image of the two bead zones with attached fluorophores can be seen in Figure 1(c). The portable imaging device is a Raspberry Pi Zero W with a camera attached, fluorescent optics, a lithium-ion battery, LEDs, and a custom peristaltic pump setup, all assembled in a 3D-printed light-tight case. This case is printed using the Objet30 Pro 3D printer and can be seen with all parts assembled in Figure 2.

Saliva samples were collected from human participants with approval from Cornell's Institutional Review Board, and then stored at 4°C until analysis. These samples were analyzed using a commercial ELISA kit to determine the concentration of cortisol in each. These samples were also filtered using a custom 3D-printed filter setup (Figure 3) and then flowed through the microfluidic chips and imaged. Some preliminary results from some samples can be seen in Figure 4.

References:

[1] Kirschbaum C, Hellhammer DH Salivary cortisol in psychoneuroendocrine research: recent developments and applications. Psychoneuroendocrinology, 1994 - Elsevier.

[2] Umeda T, Hiramatsu R, Iwaoka T, et al. Use of saliva for monitoring unbound free cortisol levels in serum. Clin Chim Acta 110:245-253. doi: 10.1016/0009-8981(81)90353-3 (1981).

An *in vacuo* Microfluidic Mixer for Biological X-Ray Solution Scattering

CNF Project Number: 1940-10

Principal Investigator(s): Richard E. Gillilan

User(s): Christopher Flynn

Affiliation(s): Macromolecular Diffraction Facility of the Cornell High Energy Synchrotron Source (MacCHESS); Cornell High Energy Synchrotron Source; Department of Physics, Fort Lewis College, Durango, Colorado

Primary Source(s) of Research Funding: National Institutes of Health GM-103485

Contact: reg8@cornell.edu, csflynn@fortlewis.edu

Website: www.macchess.cornell.edu/MacCHESS/bio_saxs.html

Primary CNF Tools Used:

Abstract:

Small angle x-ray scattering (SAXS) is an important tool for probing the structure and interactions of biological molecules under realistic physiological-like conditions. Fabrication of plastic microfluidic chips for time resolved small angle x-ray solution scattering (TR-SAXS) involves embedding various thin, fragile x-ray transparent window materials within a polymer matrix. This continuous-flow mixer utilizes chaotic laminar flow that is designed to reach multiple timescales down to a millisecond. High flow rates of water-based samples though the cell induces high pressures that present design challenges. Our current cell design utilizes relatively deep 500 µm channels for fluid flow combined with either polyimide or synthetic mica x-ray windows. Synthetic mica is more rigid than polyimide, resulting in less flexing of x-ray windows under pressure. Mica also has the advantage of fewer x-ray scattering artifacts and its hydrophilic nature lends itself to bonding.

Summary of Research:

Biological small angle x-ray solution scattering (BioSAXS) is a popular technology for extracting structural information from biomolecules under realistic physiological-like solution conditions. Given that many studies in structural biology today rely heavily on crystalline and/or frozen samples, the ability to probe solution behavior is more critical than ever. Many important biological phenomena change on times scale ranging from 1 ms to several seconds [1]. Time-resolved SAXS methods have been developed in the literature that can reach these timescales, but the techniques are difficult to implement and still require intensive effort by specialists in the field. High-volume, repeated experiments required for use in a general user facility are currently impractical. The focus of this work is to make TR-SAXS more easily accessible to the general biology community by developing disposable microfluidic mixing cells that can be easily replaced to handle the high-volume, continuous duty of a user facility.

Our fabrication method uses the recently developed SUEX film (DJ Microlaminates, Sudbury, MA) to create a 500 µm thick layer containing deep microfluidic channels (Figure 1a). The x-ray window is bonded to a poly(methyl methacrylate) (PMMA) base using epoxy then overlaid with SUEX, exposed and developed by standard photolithography techniques. A second x-ray window (4, in Figure 1B) covering all the liquid channels, is sandwiched between the underlying SUEX layer and an outer PMMA support. While thin 7 µm polyimide has been used for some time in x-ray work, it is easily deformed resulting in irreproducible scattering absorption and undesirable scattering background. High quality synthetic mica is now available with superior rigidity and low background scatter (fluorophogopite, Great Wall Mineral, Shijiazhuang, China). Bench testing subjected layers to pressures of approximately 4500 bar, though pressure downstream of the mixing zone was estimated to be much lower (130-70 mbar).

References:

[1] Panine, P., S. Finet, T. M. Weiss and T. Narayanan (2006). "Probing fast kinetics in complex fluids by combined rapid mixing and small-angle x-ray scattering." Advances in Colloid and Interface Science 127(1): 9-18.

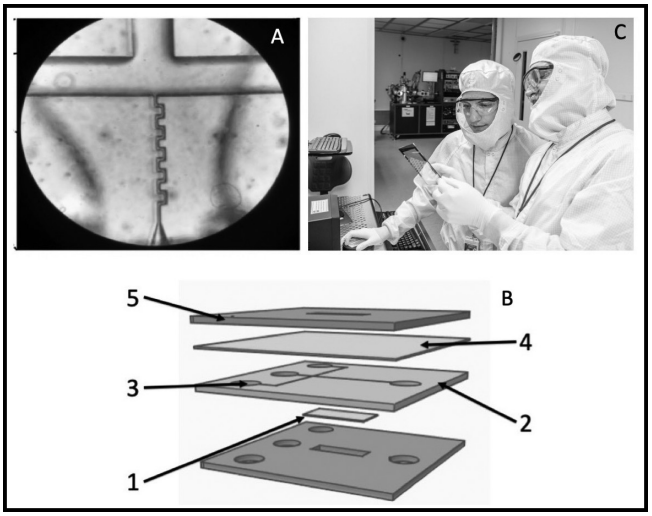

Figure 1: Microfluidic TR-SAXS chip. (A) Closeup view of mixing region. (B) Schematic of layer design: 1. x-ray window, 2. SUEX layer, 3. Input port, 4. x-ray window, 5. PMMA layer. (C) Christopher Flynn, Fort Lewis, Colorado, SunRise program for Summer students, together with CHESS scientist Richard Gillilan examining their latest photolithography mask.

Biomechanics of Bacteria

CNF Project Number: 1970-10

Principal Investigator(s): Christopher J. Hernandez

User(s): Christine E. Harper, Melanie F. Roberts

Affiliation(s): Sibley School of Mechanical and Aerospace Engineering, Meinig School of Biomedical Engineering; Cornell University

Primary Source(s) of Research Funding: National Science Foundation 1463084

Contact: cjh275@cornell.edu, ceh272@cornell.edu, mfr75@cornell.edu

Website: hernandezresearch.com

Primary CNF Tools Used: ASML, Oxford 100, AJA sputter deposition, VersaLaser, MOS clean anneal

Abstract:

The mechanical properties of the bacterial cell envelope influence cell growth, cell division and subcellular localization of membrane proteins. Here we demonstrate the ability to apply mechanical loads to live bacteria, the first step toward determination of mechanical properties of bacterial components *in vivo*. Additionally, we show that devices based on the same concept have the ability to separate bacterial species/strains from one another based on the cell mechanical phenotype.

Summary of Research:

In bacteria, the ability to resist mechanical forces is necessary for survival and growth, allowing cells to withstand osmotic pressures while maintaining cell shape, cell growth and division. Hence, the mechanical properties of bacteria and bacterial structural components influence species competition and resistance to toxins and antibiotics. Our work involves the use of micro/nano fabricated devices as tools for mechanical testing of live bacteria. Within our devices individual bacteria are flowed into tapered channels and trapped. The point at which the cell becomes trapped reflects the whole cell stiffness, more stiff cells are trapped earlier in the channels and less stiff cells are able to travel further in to the channels (Figure 1).

Key advantages of this microfluidic platform for profiling the biomechanical properties of bacteria include: minimal sample preparation, no chemical immobilization or labeling, and the ability to analyze hundreds of cells at once.

In our first series of experiments we manufactured devices on silica glass wafers using deep UV photolithography to achieve nano-scale features (250 nm smallest dimension). These glass on glass devices were manufactured using the ASML, Oxford 100, AJA sputter deposition, VersaLaser, and MOS clean anneal tools at the Cornell NanoScale Science and Technology Facility.

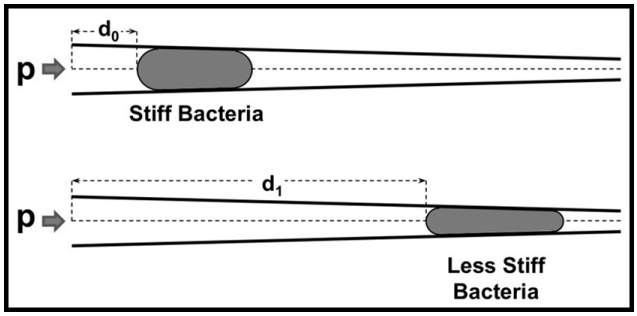

Figure 1: Bacteria under fluid pressure (p) are forced into tapered channels. The distance a cell travels into a tapered channel depends on cell stiffness with more compliant cells traveling further into the channels. The distance traveled by a cell into the tapered channel (d1) is therefore an indicator of cell stiffness. Viewing the deformation of a cell under two different applied pressures can be used to determine the mechanical properties of the cell envelope.

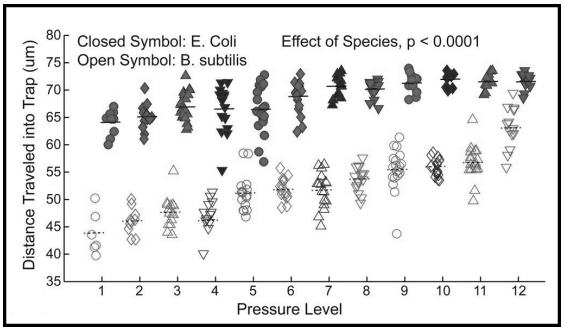

Figure 2: The position of bacteria occupying trap channels at twelve different pressure levels (where level 1 is lowest and level 12 is greatest) in a single experiment are shown. Horizontal lines indicate averages at each pressure level. E. coli *travel further into the traps than* B. subtilis *overall ($p < 0.0001$, ANCOVA) as well as at each individual pressure level ($p < 0.0001$, t tests). (Find full color on pages xiv-xv.)*

In the first device design bacteria in liquid culture were submitted to up to 12 different applied pressures to establish the biomechanical profile of two model organisms, *E. coli* and *B. subtilis*.

Our results demonstrated differences in stiffness between *E. coli* and *B. subtilis* (Figure 2) and suggested that a device with a shorter channel length would allow transport of *E. coli* but not *B. subtilis*, potentially allowing for separation of bacteria based on the biomechanical properties [1]. When combined with theoretical mechanics models, it allowed us to determine the stress distribution within individual bacteria and study their response to mechanical stimulation [2].

In our recent work we have explored the effects of mechanical loads on the assembly/disassembly of multicomponent efflux pumps. Multicomponent efflux pumps are three-part channels that cross the inner membrane, periplasm and outer membrane of bacteria and are used to remove toxins including excessive metal ions and antibiotics. Our data suggests that the assembly and function of multicomponent efflux pumps is sensitive to mechanical stress and strain. Increased octahedral shear stress due to increased pressure in our microfluidic device was shown to promote disassembly of multicomponent efflux pumps as well as decreasing cell elongation rate (Figure 3), suggesting metal resistance of mechanically stressed cells may be reduced [4].

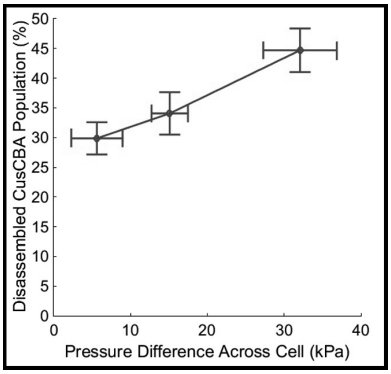

Figure 3: Bacteria trapped within tapered channels experience a difference in pressure across the cell length. Increased pressure difference across the cell was shown to increase disassembly of the multicomponent efflux pump CusCBA.

References:

[1] Sun, X., Weinlandt, W.H., Patel, H., Wu, M., Hernandez, C.J. (2014) "A Microfluidic Platform for Profiling Biomechanical Properties of Bacteria." Lab Chip. 14 (14), 2491-2498. NIHMS600175.

[2] M. F. Roberts, A. Srivastava, X. Sun, L. Kreminski, L. Ling, L. Wang, P. Chen, C-Y. Hui, C. J. Hernandez. "A Microfluidic Platform for Generating Non-Uniform Mechanical Stress in Cell Envelopes of Live Bacteria," American Society of Microbiology Annual Meeting. Boston, MA, USA. 2016.

[3] M.F. Roberts, A. Srivastava, L.M. Wang, C-Y Hui, L.A. Genova, P. Chen, C.J. Hernandez, "A microfluidic system for mechanical characterization and stimulus of individual bacteria," European Society of Biomechanics 2017.

[4] L.A. Genova, M.F. Roberts, Y.C. Wong, C.E. Harper, A.G. Santiago, B. Fu, A. Srivastava, W. Jung, L.M. Wang, Krzemiski, X. Mao, X. Sun, C.Y. Hui, P. Chen, C. J Hernandez. "Mechanical stress compromises multicomponent efflux complexes in bacteria". BioRxiv preprint 2019.

Design and Application of Microfluidic Devices to Study Cell Migration in Confined Environments

CNF Project Numbers: 2065-11
Principal Investigator(s): Jan Lammerding
User(s): Aaron Windsor

Affiliation(s): Meinig School of Biomedical Engineering, CNF, Weill Institute; Cornell University

Primary Source(s) of Research Funding: National Institutes of Health award R01 HL082792; National Institutes of Health award 1U54 CA210184; Department of Defense Breast Cancer Research Program Breakthrough Award BC150580; National Science Foundation CAREER award CBET-1254846

Contact: jan.lammerding@cornell.edu, ajw49@cornell.edu

Website: http://lammerding.wicmb.cornell.edu/

Primary CNF Tools used: Heidelberg DWL 2000 mask writer, ABM contact aligner, SÜSS MA6 contact aligner, Plasma-Therm 770, Anatech SCE-110-RF resist stripper, Trion Minilock III ICP etcher, Tencor P-10 profilometer, MVD

Abstract:

For multicellular organisms, cell migration can act as a double-edged sword. While being vital for embryonic development, wound healing, and immune responses, wayward cells may also disrupt essential biological processes that can detrimentally affect the long-term survival of a life form. This is particularly true for the ability of metastatic cancer cells to translocate from the primary tumor, invade into surrounding tissues, and colonize distant organs. Metastatic cancer cells are able to penetrate through tight interstitial spaces of only 1-30 µm in diameter. The squeezing through such confined spaces places substantial physical stress on the cell nucleus, leading to nuclear envelope ruptures, chromatin herniation, and significant DNA damage. To study these processes in more detail, we created a microfluidic device that models the tight 3D constrictions that metastatic cancer cells may encounter during the metastatic process. The device gives us a high-throughput method for observing the short- and longer-term effects mechanically induced nuclear deformation has on the tumor cells. Originally, we constructed our intricate PDMS microfluidic devices from SU-8 molds, which lacked reliability and inconsistently reproduced the most critical features of our designs. Thus, we shifted the nanofabrication process to deep-reactive-ion etching (DRIE) and reactive-ion etching (RIE) of silicon. This revised approach has enabled us to improve the fidelity of our critical features, while also reducing the fabrication time and costs. The precision of silicon etching has opened doors for creating more complex microfluidic designs and other novel ideas. For example, we recently created a set of five devices that mimic different densities of the extracellular collagen fiber networks that form in many tissues. These devices are now finding use in the study of cancer cell migration and immune cell motility in confined spaces. We also have explored the use of fluorinated ethylene propylene (FEP Teflon®) as a substitute for PDMS molded devices. Nanoimprinted FEP has a reflective index near that of water and could give our devices the capability of super-resolution microscopy. Taken together, these examples illustrate new uses of the available nanofabrication technologies to create improved *in vitro* models to study cancer cell migration.

Summary of Research:

For decades, cell biologists have relied on two-dimensional (2D) migration assays for their convenience and seamless integration with many common imaging tools [1]. While being impactful in the field of cell biology, 2D studies are limiting for studying cancer cell migration [2], as they do not accurately depict how a cancer cell moves *in vivo* [3]. In order for cells to move throughout the body, they must navigate three-dimensional (3D) matrixes of different compositions, pore sizes and stiffnesses. Our goal was to design polydimethylsiloxane (PDMS) based microfluidic devices that recreate the confining 3D environment cells encounter *in vivo*, using approaches that provide precisely controlled and consistent geometries, and that enable high resolution imaging of the cells as they migrate through the devices [4]. These devices support a wide range of cell lines, and enable high-quality fluorescence imaging of nuclear lamina bucking, chromatin strain, DNA damage and nuclear rupture/blebbing and repair [4,5].

Over the past two years, we have explored alternate nanofabrication methods for the microfluidic migration devices. SU-8 was effective in creating these migration devices, but suffered from a few common fabrication issues. First, the reproducibility of the fine (~1 µm) features was difficult to achieve consistently, which led to an overuse of the few successful device wafers. The repeated molding and removal of PDMS would overtime weaken the SU-8/silicon substrate bond, eventually resulting in the delaminating of features and device failure. In order to reliably reproduce and preserve our most critical features, we decided to forgo SU-8 and instead etch the fine constrictions of the devices directly into the silicon substrate. We accomplished this "bottom-down" approach by using a negative photoresist mask and deep-reactive ion etching (DRIE). Not only were the critical dimension sizes reproduced with fidelity (Figure 1), but the fabrication time was cut in half.

Another advantage to this process was the ease of creating 1 µm features through contact lithography with photoresist compared to SU-8. With this in mind, we revisited some of our alternative migration device designs. One design that was now achievable with DRIE was creating large (~25 mm × 25 mm) arrays of randomly spaced 5 µm diameter circular pillars, mimicking collagen matrixes with different densities (Figure 2). While the

DRIE process successfully created the desired geometries, we noticed that the holes etched into the silicon wafer to mold the 5 µm PDMS pillars frequently contained remnants of the PDMS pillars after molding. We determined that the scalloped-sidewalls from the DRIE etch likely contributed to this problem, and that smoother sidewalls were required to facilitate removal of the PDMS replicas. To achieve this, we developed a reactive-ion etching (RIE) protocol, which was subsequently used for all device fabrication. The photonics etch on the Plasma-Therm Unaxis SLR 770 was chosen for its unique capability to produce smooth anisotropic sidewalls in silicon and compatibility with our original DRIE lithography. As another demonstration of the versatility of the new RIE approach, we created another migration design for the observation of single cells passing a precisely defined constriction (Figure 3). We highly recommend this process to other researchers aiming to produce microfluidic devices with smooth walls, feature heights of several micrometers, and width in the sub-micrometer range.

Another major breakthrough this past year was discovering a method to remove SU-8 features from silicon wafers, which enables reusing wafers when the SU-8 structures have become damaged after repeated use. The weakest point to any SU-8 device is its substrate adhesion, especially after repeated PDMS molding. For our migration devices, the silicon wafers contain the fine featured etched into the wafer using the RIE approach described above, and additional larger SU-8 features for the fluid handling. Typically, the wafers have to be discarded after any SU-8 component begins to delaminate from the wafer. To overcome this issue, we developed two techniques that can remove all the remaining SU-8 from our wafers while not affecting the fine photonics etch features. This approach enabled us to spin on a new layer of SU-8 and reuse the fine silicon etched wafer. Intriguingly, this process can also be used to produce and liftoff designs entirely made from SU-8 (Figure 4), which could find future use in the fabrication of small micrometer-sized parts.

Lastly, we investigated PDMS substitutes for molding our microfluidic devices for super-resolution applications that require imaging through media that matches the refractory index of water, i.e., n = 1.33 [6]. The cured PDMS typically used for microfluidic devices has a refractive index of 1.41 [7], which is not well suited for the lattice light sheet imaging. Instead, we chose to use fluorinated ethylene propylene (FEP) as an alternative material for the device fabrication. FEP is a highly transparent copolymer of hexafluoropropylene and tetrafluoroethylene with a refractive index of 1.334 (https://holscot.com/glossary/fep/), closely matching that of water. We were able to emboss thin FEP sheets with micrometer resolution and minimum damage to our existing molds with the Nanonex 2500 nanoimprint tool. The most accurate representations of our both DRIE and RIE master wafers were achieve slightly below the melting point of FEP (260°C - 265°C) (Figure 5). Ongoing work is focused on optimizing thermal or chemical bonding of FEP sheets to each other or to glass substrates to create complete microfluidic devices.

References:

[1] Wu, P., Gilkes, D. M., and Wirtz, D. Annual Review of Biophysics, 47(1), 549-567. doi:10.1146/annurev-biophys-070816-033854 (2018).

[2] Van Horssen, R. V., and Hagen, T. L. J of Cellular Physiology, 226(1), 288-290. doi:10.1002/jcp.22330 (2010).

[3] Lautscham, L., et al. Biophysical Journal, 109(5), 900-913. doi:10.1016/j.bpj.2015.07.025 (2015).

[4] Davidson, P. M., Sliz, J., Isermann, P., Denais, C., and Lammerding, J. Integrative Biology,7(12), 1534-1546. doi:10.1039/c5ib00200a (01 December 2015).

[5] Denais C.M., Gilbert R.M., Isermann P., McGregor A.L., te Lindert M., Weigelin B., Davidson P.M., Friedl P., Wolf K., Lammerding J. Science. 352(6283):353-8. doi: 10.1126/science.aad7297 2016 Apr 15.

[6] Bashkatov, A. N., and Genina, E. A. Saratov Fall Meeting 2002: Optical Technologies in Biophysics and Medicine IV,5068, 393-395. doi:10.1117/12.518857 (13 October 2003).

[7] Dow Corning Technical Data Sheet SYLGARD™ 184 Silicone Elastomer. Retrieved May 6, 2019, from https://consumer.dow.com/content/dam/dcc/documents/en-us/productdatasheet/11/11-31/11-3184-sylgard-184-elastomer.pdf?iframe=true (2017).

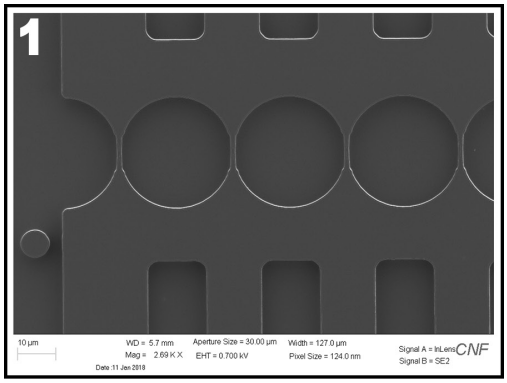

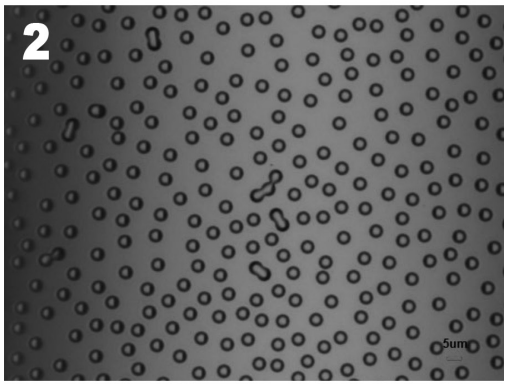

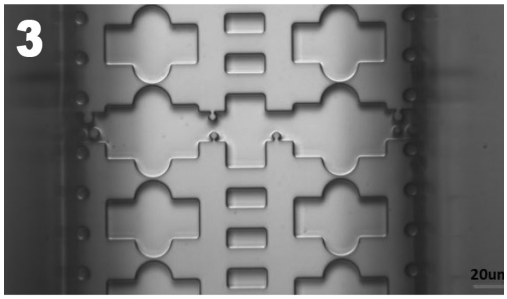

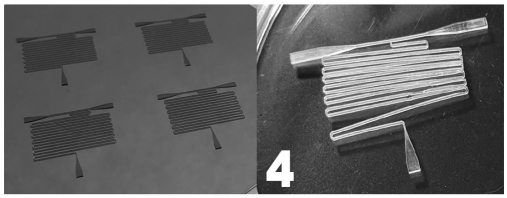

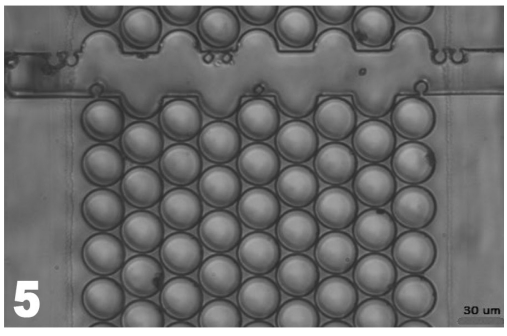

Figure 1: *SEM image of a row of 1 µm constrictions created by etching 5 µm into Si by DRIE.* ***Figure 2:*** *An example of DRIE 5 µm diameter holes intended for PDMS molding pillars to mimic collagen (50x).* ***Figure 3:*** *Single cell migration device with 1 µm constriction gaps.* ***Figure 4:*** *Left: Four SU-8 microfluidic devices ≈ 170 µm tall on a four-inch silicon wafer. Right: A microfluidic device detached from the silicon substrate.* ***Figure 5:*** *Nanoimprinted fluorinated ethylene propylene (FEP) with 5 µm DRIE master @ 265°C (20x).*

Electrochemical Lasso for Trapping Biomolecules inside Zero-Mode Waveguides

CNF Project Number: 2214-13

Principal Investigator(s): Meni Wanunu[1]

User(s): Mohammad Amin Alibakhshi[1], Fatemeh Farhangdoust[2]

Affiliation(s): 1. Physics Department, 2. Bioengineering Department; Northeastern University

Primary Source(s) of Research Funding: NIH/National Human Genome Research Institute award no. HG009186

Contact: wanunu@neu.edu, m.alibakhshi@northeastern.edu, f.farhangdoust@northeastern.edu

Website: http://www.northeastern.edu/wanunu/

Primary CNF Tools Used: Electron-beam lithography, e-beam evaporation and lift-off

Abstract:

Single molecule real time (SMRT) sequencing technology developed by Pacific Biosciences is a robust single molecule DNA sequencing method in which DNA strand replication by an individual DNA polymerase is imaged using fluorescently labeled nucleotides [1-2]. SMRT sequencing, however, suffers from inefficient loading of DNA molecules into the zero-mode waveguides (ZMWs), a sequencing unit that provides the smallest available volume for light detection. In addition, ZMWs are biased towards diffusion-based entry of short DNA templates. To overcome these challenges, our lab introduced two powerful tools, i.e., nanopore ZMW (NZMW) [3] and porous ZMW (PZMW) [4], to electrokinetically capture DNA fragments inside ZMWs. The efficiency of voltage-induced DNA loading into these waveguides is length-independent and is 6-7 orders of magnitude larger than diffusion-based SMRT sequencing. Although NZMW and PZMW are effective tools for capturing long DNAs in picogram levels, they are fabricated on top of free-standing ultrathin membranes, which makes them fragile and difficult to scale up. In this work, we introduce a new technique in order to draw DNA fragments inside ZMWs fabricated on fused silica substrates.

Summary of Research:

The working principle of our design relies on embedding metallic electrodes (platinum, Pt) under the waveguides to create an electric field. This electrode film is separated from the ZMWs made of aluminum, by a dielectric layer. Application of a voltage to the electrode layer with the use of proper electrolyte allows efficient electrophoretic DNA capture at picogram levels. Electron-beam lithography, e-beam evaporation, and lift-off are used to fabricate 100 nm ZMW arrays in wafer scale. Our new device eliminates the need for free-standing membranes and enables scaled-up fabrication, reduces the background optical noise, and improves the DNA loading efficiency by several orders of magnitude.

We have continued to fabricate these devices for DNA sequencing experiments. Figure 1 shows PtZMWs' fabrication process and Figure 2 is scanning electron microscope image of the top view and cross-section of an array of ZMWs.

References:

[1] Levene, M. J.; Korlach, J.; Turner, S. W.; Foquet, M.; Craighead, H. G.; Webb, W. W., Zero-mode waveguides for single-molecule analysis at high concentrations. science 2003, 299 (5607), 682-686.

[2] Eid, J.; Fehr, A.; Gray, J.; Luong, K.; Lyle, J.; Otto, G.; Peluso, P.; Rank, D.; Baybayan, P.; Bettman, B., Real-time DNA sequencing from single polymerase molecules. Science 2009, 323 (5910), 133-138.

[3] Larkin, J.; Foquet, M.; Turner, S. W.; Korlach, J.; Wanunu, M., Reversible positioning of single molecules inside zero-mode waveguides. Nano letters 2014, 14 (10), 6023-6029.

[4] Jadhav, V.; Hoogerheide, D. P.; Korlach, J.; Wanunu, M., Porous Zero-Mode Waveguides for Picogram-Level DNA Capture. Nano letters 2018, 19 (2), 921-929.

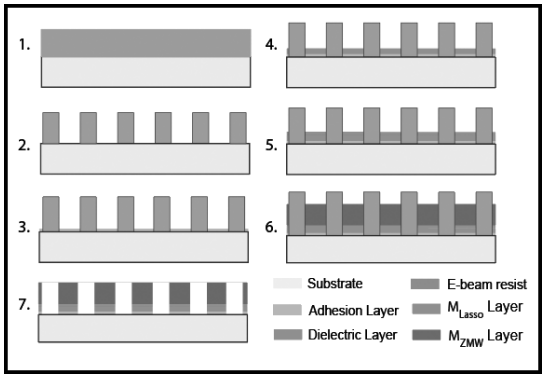

Figure 1: Schematic representation of ZMW fabrication process: 1. Spincoat negative e-beam resist and bake. 2. Expose using e-beam lithography and develop resist. 3. E-beam evaporation of an adhesion layer on the fused silica substrate, followed by deposition of Pt layer (electrode), alumina (dielectric layer), and 100 nm aluminum (cladding layer of ZMWs). 4. Lift-of-resist using 1165 stripper.

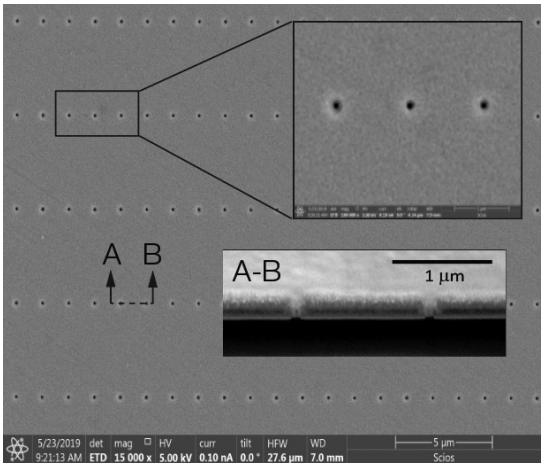

Figure 2: SEM of an array of 100 nm diameter ZMWs. Cross-section of the ZMWs shown in the bottom inset demonstrates that the cladding layer (aluminum) is separated from the electrode (Pt) by a dielectric layer (Al_2O_3).

Zero-Mode Waveguides Fabrication for DNA Nucleosome Sequencing Application

CNF Project Number: 2214-13

Principal Investigator(s): Meni Wanunu

User(s): Pengyu Zheng

Affiliation(s): Department of Physics, Northeastern University

Primary Source(s) of Research Funding: NIH/NHGRI R01

Contact: wanunu@neu.edu, zheng.p@husky.neu.edu

Website: http://www.northeastern.edu/wanunu/index.php

Primary CNF Tools Used: JEOL 6300 electron-beam lithography system

Abstract:

Cost-effective deoxyribonucleic acid (DNA) sequencing has been one of the most important goal in this era of biological and health science study. Zero-mode waveguide (ZMW) has been proven to be a promising technology for single DNA sequencing [1]. This research aims to apply this technology on directly reading DNA nucleosome sequence while detecting nucleosome modification in parallel. This could be a new innovative means of probing for epigenetics [2].

Summary of Research:

ZMW is essentially a ~ 100 nm size well that allows a confined region of laser illumination at its bottom. Once a DNA/polymerase complex is immobilized in the ZMW, the sequence can be read by imaging the incorporation of fluorescence-labeled nucleotides [1]. In our research, we plan to use it on DNA nucleosome complex instead of a simple single strand DNA. Thus the information of histone modification can be probed at the same time as we sequence the DNA, and the modification site can be located in the genome.

The proposed structure for ZMW chips is an array of ~ 100 nm holes on a thin film of aluminum on top of a glass wafer, similar to other designs under the same CNF project. We have finished a few trainings for some necessary fabrication tools, but haven't yet started the fabrication. Meanwhile colleagues Mohammad Alibakhshi and Fatemeh Farhangdoust are working on optimizing the protocol for glass wafer based ZMW fabrication.

References:

[1] Levene, M. J.; Korlach, J.; Turner, S. W.; Foquet, M.; Craighead, H. G.; Webb, W. W. Science 2003, 299, 682-686.

[2] Shema, Efrat, et al. "Single-molecule decoding of combinatorially modified nucleosomes." Science 352.6286 (2016): 717-721.

Dual-Gradient Microhabitat Platform for Microalgae Growth

CNF Project Number: 2262-13
Principal Investigator(s): Dr. Mingming Wu
User(s): Fangchen Liu

Affiliation(s): Department of Biological and Environmental Engineering
Primary Source(s) of Research Funding: United State Department of Agriculture - National Institute of Food and Agriculture
Contact: mm272@cornell.edu, FL373@cornell.edu
Website: http://biofluidics.bee.cornell.edu/
Primary CNF Tools Used: Heidelberg mask writer DWL2000, ABM contact aligner, P10 profilometer, MVD 100

Abstract:

The occurrence of harmful algal blooms (HABs) is increasing at an alarming rate worldwide, threatening water resources and aquatic ecosystems. Nutrients are known to trigger the onset of HABs and systematic investigation at cellular level is lacking. To study the combination effects of multiple nutrients on microalgae growth in a high throughput way, a dual-gradient microhabitat platform was designed, fabricated, and characterized.

Summary of Research:

Harmful algal blooms, or HABs, are serious environmental problems, where a sudden growth of algae or cyanobacteria poses threat to freshwater and marine ecosystems. HABs deteriorate drinking water quality and have huge environmental and economical costs. Nutrient enrichment is believed to be the fundamental cause of HABs, and climate change may further intensity the problem [1]. However, there lacks a quantitative/mechanistic understanding of the roles of environmental factors in the onset of HABs at cellular level. The goal of this project is to investigate the synergistic roles of multiple environmental factors in the growth of cyanobacteria.

Environmental conditions known to affect algae growth include nutrients, mainly nitrogen (N) and phosphorous (P), light intensity and temperature. These conditions are hard to control in nature, and also cannot be quantified in a high throughput way in flasks and chemostats. Previously, an high throughput array microhabitat platform has been developed in our lab that is suitable for monitoring growth of photosynthetic microbes [2]. This platform is capable of generating a stable single nutrient gradient. Using this platform, we discovered that the growth rates of *Chlamydomonas reinhardtii* in the presence of NH_4Cl gradient fit into a modified Monod kinetics model with the half saturation constant of NH_4Cl to be 1.2 ± 0.3 μM.

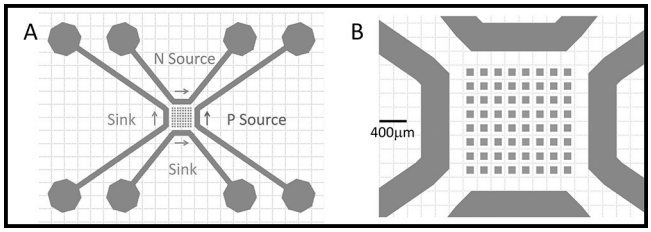

Figure 1: Dual-gradient microfluidic platform design. A. Top view of a device. B. A zoomed-in view of microhabitats and channel. The 8 × 8 array of 100 μm cubic habitats are separated by 100 μm from each other. These habitats are surrounded by four channels with width of 400 μm and height of 200 μm. N source and P source runs through the top and right channel respectively, and the other channels are sink channels. A gradient is generated for each chemical species in the microhabitat array region through molecular diffusion.

In this project, we developed a microhabitat platform that can provide dual nutrient gradients to facilitate a more realistic condition found in nature. The design of our device is shown in Figure 1, which consists of 64 microhabitats in the form of an 8 × 8 array and each habitat is 100 μm × 100 μm × 100 μm. The microhabitat array is surrounded by two sets of side channels each with the width of 400 μm and height of 200 μm. In each set of side channels, we can run source media (with N, or P) and blank media respectively, and a stable gradient can be simultaneously generated along vertical and horizontal directions.

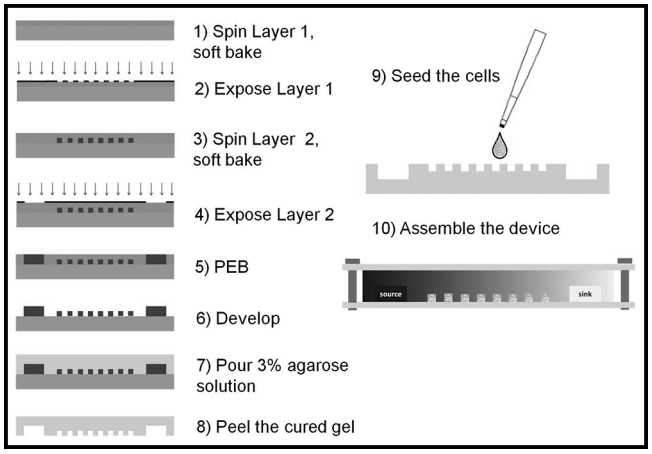

Figure 2: Schematics of a two-layer SU-8 photolithography procedure and the final microfluidic device assembly. First, a 100 µm resist layer was spun on wafer, soft baked and exposed. Then, another 100 µm layer was spun on top and baked together overnight, followed by the second exposure and post exposure bake (PEB) for the 200 µm structures. The unexposed resist was then developed and the structures went through hard bake. For device assembly, the pattern was imprinted on an agarose gel, and cells were seeded in the microhabitats. The gel was then sandwiched between glass slide and manifolds and tightened by screws.

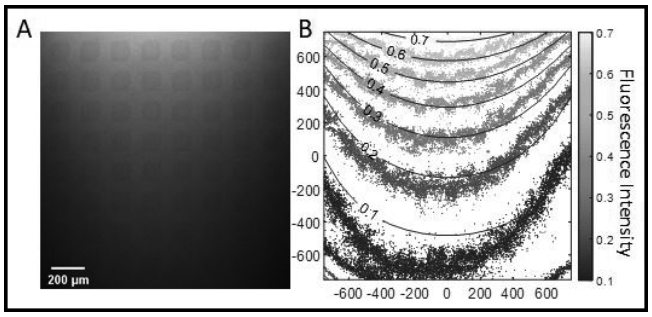

Figure 3: Characterization of the device using fluorescein (FITC) dye. A. FITC solution was introduced to top channel and buffer solution without FITC were introduced in the other three channels at t = 0. The fluorescence image is taken at the middle where the microhabitats are at t = 60 min. B: Contour plot of simulated (lines) and experimental (dots) concentration fields at t = 60 min. Concentration is scaled such that the concentration in source channel is 1 and sink channel 0.

Soft lithography was used to make this dual-gradient microhabitat platform, which involves fabricating the silicon master mold and molding the pattern onto agarose gel for device assembly. Schematics of the step by step procedure are shown in Figure 2. The silicon master mold was fabricated using two layer SU-8 negative resist photolithography, since the channels are 200 µm high and the microhabitats are 100 µm high. The post exposure bake (PEB) of the first layer of photo resist was combined with the soft bake of the second layer of the photo resist. Also, it was found that slow temperature ramping and relaxation time after each bake is critical to minimize internal stress in order to prevent resist detachment problem. After developing, the height of the feature were measured using P10 profilometer and a layer of FOTS was deposited using molecular vapor deposition (MVD100) to increase the surface hydrophobicity for easier demolding of agarose gel. To transfer the pattern, boiled 3% agarose solution was poured on the silicon master and peeled once it cured.

The gradient behavior of this dual-gradient platform was characterized using Fluorescein (FITC) dye (Figure 3). 50 µM FITC was flown through the top channel, and blank media in the other channels at t = 0, and the stable gradient was established via molecular diffusion through the agarose gel. A fluorescence image at 60 min was plotted together with results from a 2D COMSOL simulation, which uses Fick's second law for diffusion and fixed concentrations at the channels as boundary conditions. In Figure 4B, the experimental field matches the simulated concentration field, which indicates the establishment of both gradients. Currently, microalgal growth in both nitrogen and phosphorous gradient are being studied at the same time in this platform.

References:

[1] Paerl, Hans W., et al. Environmental Science and Technology (2018): 5519-5529.

[2] Kim, Beum Jun, et al. Lab on a Chip 15.18(2015): 3687-3694.

Shear-Rate Controlled Microfluidic Devices to Examine von Willebrand Factor-Mediated Platelet Deposition

CNF Project Number: 2349-15

Principal Investigator(s): Brian J. Kirby

User(s): Anjana Jayaraman, Junhyuk (Andrew) Kang

Affiliation(s): Sibley School of Mechanical and Aerospace Engineering, Cornell University

Primary Source(s) of Research Funding: NIH Project # HL089456, NSF contract # CBET-1706518

Contact: kirby@cornell.edu, aj597@cornell.edu, jk2829@cornell.edu

Website: http://blogs.cornell.edu/kirbyresearch/

Primary CNF Tools Used: ABM contact aligner, Class II resist spinners (SU-8), Heidelberg mask writer (DWL 2000), Hamatech mask chrome etch 1, resist hot strip bath, SU-8 hot plates, P10 profilometer

Abstract:

Ventricular Assist Devices (VAD) have been known to cause thrombosis, or the formation of clots in blood vessels due to the pumping of blood at high shear rates. Thrombi are formed when platelets aggregate together as a result of many blood-borne agonists and processes. The purpose of our research is to study how strain rates influence how platelets aggregate and adhere to vessel walls. We will be using microfluidic devices to mimic platelet deposition at clinically relevant shear rates, and use fluorescence microscopy to visualize the thrombi.

Summary of Research:

Our research focus has been to study VAD-related thrombosis. Thrombosis is a process by which platelets aggregate and adhere to blood vessels. This can lead to major health problems, such as nutrient deficiency, higher blood pressure, and stroke [1]. The mechanism through which platelets function is dependent on hemodynamic shear stresses [2,3].

When a ventricular assist device is implanted, it generates supra-physiological shear rates that uncoils a normally globular glycoprotein named von Willebrand Factor. When the protein chain unfolds, it reveals several binding sites that enable tethering to both collagen and platelets [2]. This tether gives platelets sufficient time and contact to collagen to activate via the GP IIb/IIIa integrin and activates the platelets, releasing more prothrombogenic biochemical agonists such as adenosine diphosphate, thromboxane A2, and thrombin [5,6]. Our group's objective is to study this mechanism using microfluidic chips made of polydimethylsiloxane (PDMS) that allow for precise strain rate control.

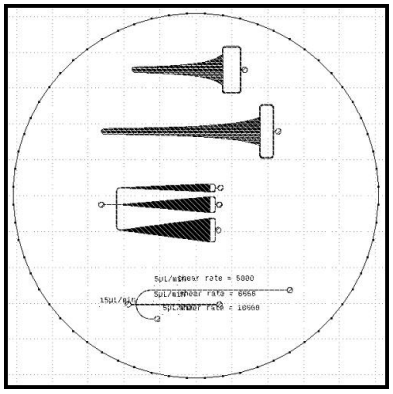

Figure 1: Computer aided design of channel geometries: (from top to bottom) short and long hyperbolic channels, expansion channels (5°, 10°, 15°), standard width channels (40 µm, 30 µm, 20 µm).

The design features three different channel geometries (Figure 1). One channel comprises a single inlet that diverges into three channels, each with a different width (40, 30 and 20 µm) in order to examine platelet deposition at a constant shear rate. Next, there are three channels that expand gradually at angles of 5°, 10°, and 15°. This design helps us study platelet deposition at constantly varying shear rates.

The third design is a hyperbolic expansion channel. We have incorporated hyperbolic channels of two different lengths; however, in both cases, along the central axis, the flow is extensionally dominated. In both the standard and hyperbolic expansions, there are square-shaped microposts that exist serve as a dual purpose of preventing channel collapse and for examining the effects of different obstacle geometries and orientations with respect to the flow direction on platelet deposition.

In order to implement our design into a device, we first used the Heidelberg DWL 2000 mask writer to generate

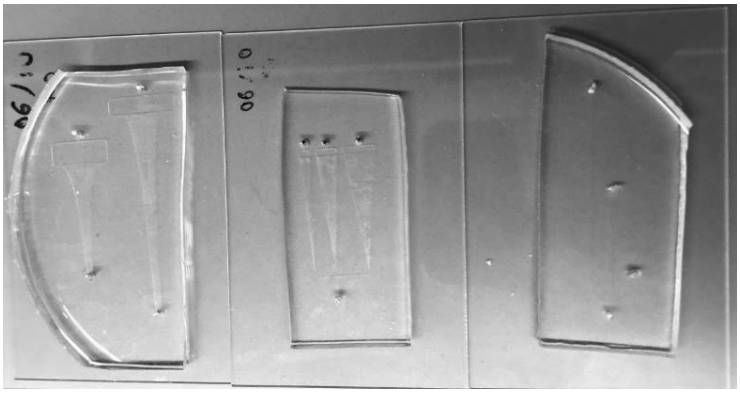

Figure 2: Microfluidic devices made of PDMS plasma bonded to glass surface.

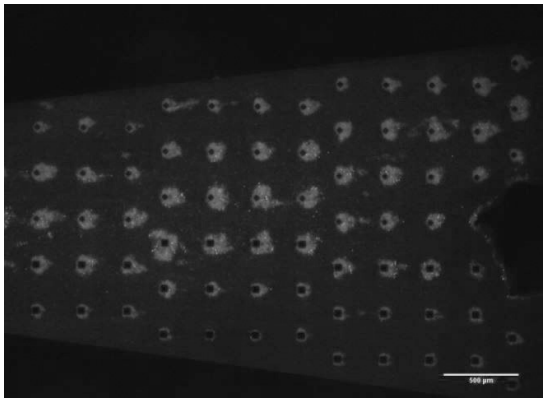

Figure 3: Mepacrine-labelled platelets depositing during perfusion through the 15° expansion channel. Flow rate is 18.8 is μL/min from left to right.

our microfluidic channel design on a chrome-coated glass plate. The chrome sputtered layer was etched on the chrome using the Hamatech Mask Chrome Etch 1, and the resist was stripped using a strip bath. In the class II photolithography room, we spin-coated SU-8 photoresist to a thickness of 50 μm. Bake times and exposure times were calculated based on recommendations provided by experienced CNF personnel [7]. We used the ABM contact aligner with our patterned chrome-coated plate and SU-8 coated wafer to expose the channel features onto the wafer. Following a post-exposure bake and SU-8 developer bath, the features were generated on the silicon wafer. Finally, to check our feature dimensions, we used the P10 profilometer to check the channel thickness.

In order to turn this wafer into a usable device, we poured a 9:1 mixture of Dow Corning Sylgard 184 silicone elastomer and curing agent onto the wafer and used a vacuum pump to create a bubble-free, rigid set of channels. The PDMS was then baked in an oven at 60°C for 150 minutes. Finally, the devices were plasma bonded onto glass slides.

In order to use these devices for imaging platelet deposition, we mix citrated ovine whole blood with mepacrine, a fluorophore taken up by platelets that allows them to be visualized using fluorescent light. We coat the channels with a collagen solution to create a thrombogenic surface so that the platelets can adhere to the glass. In our preliminary work, we have flowed blood through the channels at a constant flow rate and observed platelet deposition over several minutes (Figure 3).

References:

[1] Eckman, P. M., and John, R. Bleeding and Thrombosis in Patients With Continuous-Flow Ventricular Assist Devices. Circulation. https://doi.org/10.1161/circulationaha.111.040246 (2012).

[2] Casa, L. D. C., Deaton, D. H., and Ku, D. N. Role of high shear rate in thrombosis. Journal of Vascular Surgery. https://doi.org/10.1016/j.jvs.2014.12.050 (2015).

[3] Selgrade, B. P., and Truskey, G. A. Computational Fluid Dynamics Analysis to Determine Shear Stresses and Rates in a Centrifugal Left Ventricular Assist Device. Artificial Organs. https://doi.org/10.1111/j.1525-1594.2011.01416.x (2012).

[4] Yang, F., Kormos, R. L., and Antaki, J. F. High-speed visualization of disturbed pathlines in axial flow ventricular assist device under pulsatile conditions. Journal of Thoracic and Cardiovascular Surgery. https://doi.org/10.1016/j.jtcvs.2015.06.049 (2015).

[5] Maxwell, M. J., Westein, E., Nesbitt, W. S., Giuliano, S., Dopheide, S. M., and Jackson, S. P. Identification of a 2-stage platelet aggregation process mediating shear-dependent thrombus formation. Blood. https://doi.org/10.1182/blood-2006-07-028282 (2007).

[6] Kragh, T., Schaller, J., Kertzscher, U., Affeld, K., Reininger, A., and Spannagl, M. Platelet adhesion, aggregation, and embolism on artificial surfaces in non-parallel blood flow. Microfluidics and Nanofluidics. https://doi.org/10.1007/s10404-015-1557-5 (2015).

[7] Cornell NanoScale Facility. SU-8 Processing Suggestions [PDF file]. Retrieved from https://www.cnfusers.cornell.edu/sites/default/files/Equipment-Resources/SU8%20processing%20suggestions.pdf (2013).

Handheld Chem/Biosensor Combining Metasurfaces and Engineered Sensor Proteins to Enhance Surface Plasmon Resonance (SPR)

CNF Project Number: 2430-16

Principal Investigator and User(s): Lori Lepak

Affiliation(s): Phoebus Optoelectronics, LLC

Primary Source(s) of Research Funding: Department of Defense

Contact: llepak@phoebusopto.com

Website: www.phoebusopto.com

Primary CNF Tools Used: DWL2000 photomask writer, ASML DUV stepper, SC4500 evaporators, Oxford 81 etcher, Zeiss SEM, DISCO dicing saw

Abstract:

Since 2003, Phoebus Optoelectronics has enabled custom R&D solutions in the fields of Plasmonics, Metamaterials, Antennas, and Sensors. We work closely with our customers throughout device development, from prototype realization to small volume manufacturing. Our R&D portfolio spans the spectral ranges of visible light, infrared, terahertz, and microwave radiation, for applications in high resolution infrared imaging systems, wavelength and polarization filtering, tunable optical components, beam forming and steering, solar cells and renewable energy devices, and chemical and biological toxin sensors. Our agile team makes extensive use of the resources at the CNF for our nano/micro fabrication and testing, to provide cost efficiency and rapid turnaround.

In the present report, we discuss recent efforts to develop a chem/bio toxin detection system, which provides the state-of-the-art sensitivity of a typical benchtop system with the superior SWaP performance of a handheld system. Our surface plasmon resonance (SPR)-based sensor is expected to be capable of detecting ng/mL concentrations of selected toxins in under five minutes.

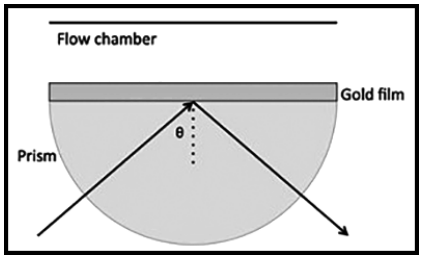

Figure 1: Surface plasmon resonance spectroscopy schematic. Reproduced from reference [8].

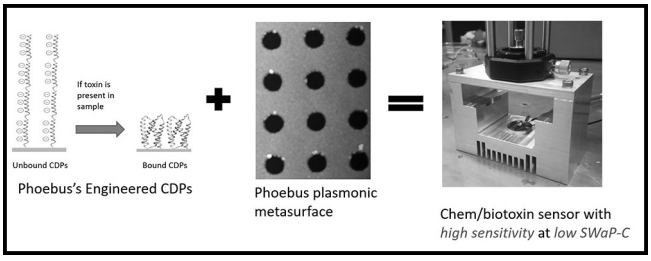

Figure 2: Phoebus-engineered sensor system combines; (a) Designed CDPs that undergo extreme conformational changes upon binding target, (b) Gold metasurface, patterned to maximize transmission at SPR resonant wavelength into (c) a high sensitivity, low SWaP-C chem/biotoxin sensor system.

Summary of Research:

SPR is a highly sensitive, label-free optical detection technique, whose underlying physics is illustrated in reflection mode in Figure 1. A laser passes through a prism, at an incident angle θ, on a gold film which is in contact with an analyte solution on its opposite side. The illumination produces an evanescent wave (surface plasmon), which significantly reduces the reflectance at a resonant angle. The resonant angle is strongly dependent on the local refractive index, within a few tens of nanometers of the gold surface, and thus is extremely sensitive to enzyme-substrate or antibody-antigen binding events near the surface. The resonance is independent of the geometric configuration of the optical elements (see [8] for mathematical derivation.), such that these results also apply to devices that operate in transmission mode.

As illustrated in Figure 2, Phoebus has combined two recently developed technologies to enable an SPR sensor system that provides enhanced sensitivity at lower SWaP, relative to technologies currently on the market.

First, Phoebus detects toxins using Computationally Designed Proteins (CDP's), engineered to undergo an exceptionally large conformational change upon binding their specific target. This conformation change increases the density of the protein layer, thereby locally increasing the effective refractive index, which in turn enhances the SPR signal by a factor of 1000x competing systems.

Second, Phoebus uses the resources of the CNF to fabricate plasmonic chips patterned with a metamaterial surface to enable Extraordinary Optical Transmission (EOT), a phenomenon unique to metastructures in which light is transmitted through apertures much smaller than the incident wavelength, at anomalously large intensities relative to the predictions of conventional aperture theory. EOT was first observed by T.W. Ebbesen in 1998 [1]. Since its founding in 2003, Phoebus has successfully harnessed EOT by incorporating metasurfaces into devices used to perform light filtering [2-3], photon sorting [4-5], polarimetric detection [6], high speed optical detection [7], and most recently, in our SPR plasmonic sensor chips [8].

These two innovations are combined by attaching the engineered CDP's to the patterned gold metasurface using standard thiol-based attachment chemistry, to make a disposable sensor chip. As shown in Figure 3, this chip is inserted into the complete 3D printed module. All of the optical elements are already assembled in-line as indicated, for a transmission based detection system. Except for Phoebus's disposable sensor chip, all of the optical components are inexpensively commercially available, which helps to make our overall system a highly cost-effective toxin sensing solution.

Our most recent generation of metasurface chips, shown in a scanning electron microscope (SEM) image in Figure 4, consist of an array of holes in a gold film, which serve both to bind the CDPs and to undergo SPR. To make the chip, we patterned the wires using the ASML deep ultraviolet photolithography system, evaporated Cr/Au, and performed a liftoff. This process is capable of consistently producing holes down to ~ 200 nm in diameter, with smooth enough sidewalls for an operable optical device.

References:

[1] Ebbesen, T.W., et al., "Extraordinary optical transmission through sub-wavelength hole arrays." Nature, (1998). 391(6668): p. 667-669.

[2] Crouse, D. "Numerical modeling and electromagnetic resonant modes in complex grating structures and optoelectronic device applications." Electron Devices, IEEE Transactions on 52.11 (2005): 2365-2373.

[3] Crouse, D., and Keshavareddy, P. "Polarization independent enhanced optical transmission in one-dimensional gratings and device applications." Optics Express 15.4 (2007): 1415-1427.

[4] Lansey, E., Crouse, D., et al. "Light localization, photon sorting, and enhanced absorption in subwavelength cavity arrays." Optics Express 20.22 (2012): 24226-24236.

[5] Jung, Y.U; Bendoym, I.; Golovin, A.B.; and Crouse, D.T. "Dual-band photon sorting plasmonic MIM metamaterial sensor." Proc. SPIE 9070, Infrared Technology and Applications XL, 90702X (June 24, 2014); doi:10.1117/12.2050620.

[6] Crouse, D., and Keshavareddy, P. "A method for designing electromagnetic resonance enhanced silicon-on-insulator metal-semiconductor-metal photodetectors." Journal of Optics A: Pure and Applied Optics 8.2 (2006): 175.

[7] Mandel, I.; Gollub, J.; Bendoym, I; Crouse, D. Theory and Design of A Novel Integrated Polarimetric Sensor Utilizing a Light Sorting Metamaterial Grating. Sensors Journal, IEEE, (2012): Vol. PP, 99

[8] Lepak, L., et al. "Handheld chem/biosensor using extreme conformational changes in designed binding proteins to enhance surface plasmon resonance (SPR)" Proc. SPIE 9862, Advanced Environmental, Chemical, and Biological Sensing Technologies XIII, 9862-7 (April 17, 2016); doi:10.1117/12.2222305.

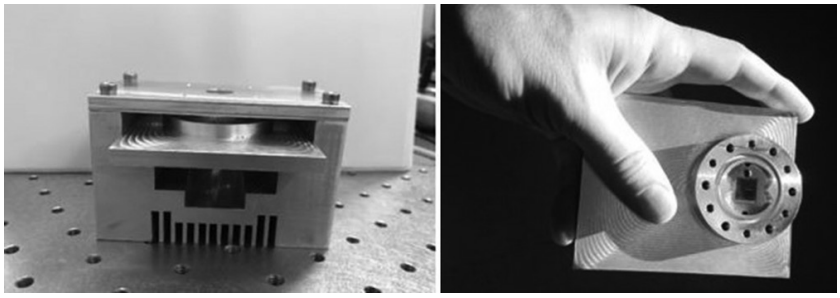

Figure 3: a) Complete Phoebus handheld biosensor system, b) removable module with plasmonic chip.

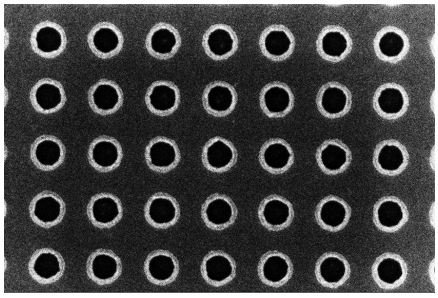

Figure 4: SEM image of a metasurface used in disposable biosensor chip.

Metasurface Enhanced Infrared Spectroscopy for Live Cells

CNF Project Number: 2472-16
Principal Investigator(s): Gennady Shvets
User(s): Steven He Huang, Junlan Lu, Robert Delgado

Affiliation(s): Applied and Engineering Physics, Cornell University
Primary Source(s) of Research Funding: Cornell University internal funding
Contact: gs656@cornell.edu, hh623@cornell.edu, jl3286@cornell.edu, rd377@cornell.edu
Website: http://shvets.aep.cornell.edu
Primary CNF Tools Used: JEOL 9500, SC4500 evaporator, Zeiss Supra SEM, PDMS casting station, Anatech resist strip

Abstract:

Infrared (IR) spectroscopy is a powerful tool for biological analyses since it is a label-free, non-invasive technique that provides information on molecular composition. IR spectroscopy of live cells, however, remains challenging due to the strong attenuation of mid-IR light in water. In our lab, we are investigating the use of metasurface-enhanced infrared spectroscopy (MEIRS) to measure live cells in cell culture. The cells are grown on a nanoplasmonic metasurface and we utilize the strong near-field hotspot of the plasmonic nanoantennas to collect IR spectra from the cells. We have demonstrated the spectral imaging of cells adhered on the metasurface as well as spectroscopically probing the response of the cells to different drugs.

Summary of Research:

Infrared (IR) spectroscopy, in which materials are identified through their molecular vibration fingerprints, has a wide range of applications in chemistry, geology, and material sciences. Applied to biological tissues, IR spectroscopy can be used as a histology or cytopathology tool, identifying tumor tissues from normal tissues and looking at the effect of chemotherapeutics on cancer cells. We have developed a new technique, using surface-enhanced infrared absorption (SEIRA) from plasmonic metasurfaces to probe the IR absorption of biomolecules and cells. This technique, which we named metasurface-enhanced infrared spectroscopy (MEIRS), had been used to measure protein monolayers [1], as well as fixed cancer cells [2]. Our current work involves further extending this technique to the measurement of live cells grown on the metasurface, in particular focusing on the spectroscopic investigation of different drugs and stimuli on these cells.

We fabricate our plasmonic metasurface in the CNF cleanroom. Starting from an IR-transparent CaF_2 substrate, we define the patterns on poly(methyl methacrylate) (PMMA) using electron-beam lithography with the JEOL 9500 system. This is followed by gold evaporation and lift off in acetone to create a working metasurface device. Scanning electron microscopy (SEM) image of our plasmonic metasurface is shown in Figure 1. In order to grow the cells on this metasurface and deliver different drugs as needed, we use a polydimethylsiloxane (PDMS) microfluidic cell culture, which is also fabricated at the CNF.

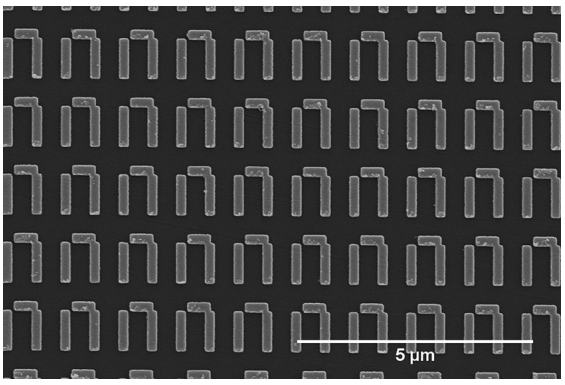

Figure 1: SEM micrograph of the plasmonic metasurface. The metasurface nanoantennas are fabricated in an array covering approximately 250 µm × 250 µm. These nanoantennas are designed to have specific optical resonances, matching the molecular vibrations of the biomolecules of interest (primarily lipids and proteins). Scale bar: 5 µm.

To measure live cells, the metasurface is treated with fibronectin and the cells are initially seeded on the metasurface in a multi-well dish. After the cells are adhered on the metasurface, the metasurface is assembled on a PDMS microfluidic cell culture chamber and measured in reflection mode with an IR microscope coupled to a Fourier Transform IR (FTIR) spectrometer. Our plasmonic metasurface has optical resonances in the

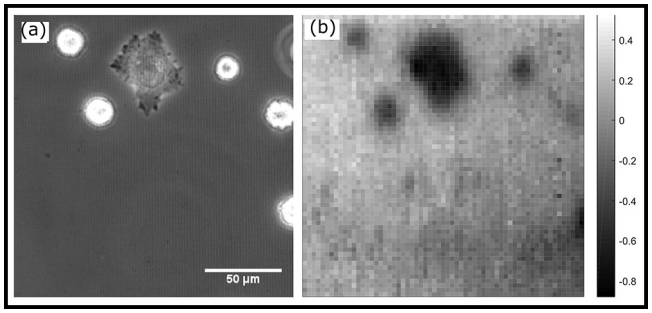

Figure 2: IR spectroscopic imaging using MEIRS combined with a focal plane array detector. (a) Phase contrast microscopy of HeLa cells grown on a metasurface. (b) The same metasurface imaged through MEIRS. The score of a principal component from PCA is plotted here. The MEIRS image reflects the cell's adhesion to the metasurface. Scale bar: 50 µm.

mid-IR, and when probed by IR light, it generates intense plasmonic "hotspots" in the vicinity of these plasmonic nanoantennas, with a penetration depth of 50-100 nm into the surrounding. Sensing cells with our metasurface relies on the spatial overlap between the cells and these plasmonic hotspots, and thus our signal is very sensitive to the degree of cell adhesion on the metasurface. Figure 2 shows a comparison between an image of HeLa cells on the metasurface obtained with phase contrast microscopy and the same cells imaged through MEIRS using an IR focal plane array detector. The MEIRS image was obtained by processing the spectra using principal component analysis (PCA). The distribution and morphology of the cells seen with the two techniques agree well, and this demonstrates that we can clearly see cells adhered on the metasurface through MEIRS.

We have applied MEIRS to the study of chemotherapeutic drugs on cancer models. Here, we measured the spectroscopic response of feline carcinoma cells to four drug combinations, control (no drug), salinomycin, doxorubicin, and a combination of both salinomycin and doxorubicin. Salinomycin is a known inhibitor of multidrug resistance protein 1 in cancer cells, and although it does not lead to high cytotoxicity alone, it increases the potency of doxorubicin when administered in combination. Figure 3 shows the MEIRS spectra measured from these cells after 2-days drug treatment. Cells treated with the combination treatment had much lower IR absorption due to proteins and lipids, and this is attributed to the cell detachment from the metasurface caused by doxorubicin-induced apoptosis. This result agrees with what we expect from salinomycin acting as a sensitizer for doxorubicin. The spectra were further analyzed by PCA and the score plot for the 1st and 2nd principal components (PCs) is shown in Figure 4. From the PCA score plot, clear separation between the cells with different treatment can be seen, even for treatments that do not significantly affect cell viability (control vs. salinomycin).

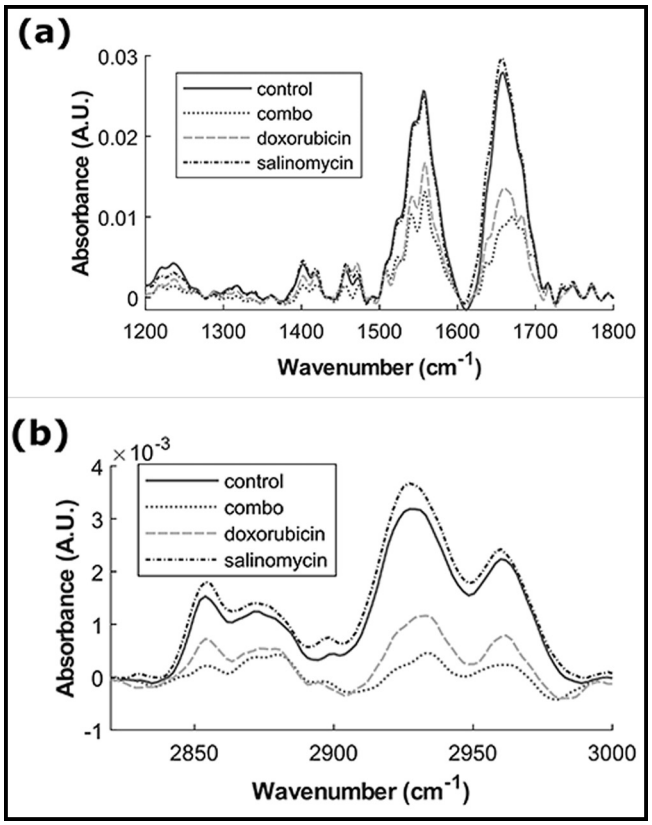

Figure 3: MEIRS spectra for feline carcinoma cells with different drug treatments. (a) Fingerprint region and (b) Lipid absorption region.

References:

[1] Wu, C., et al. Fano-resonant asymmetric metamaterials for ultrasensitive spectroscopy and identification of molecular monolayers. Nat. Mater. 11, 69-75 (2011).

[2] Kelp, G., et al. Application of metasurface-enhanced infra-red spectroscopy to distinguish between normal and cancerous cell types. Analyst 144, 1115-1127 (2019).

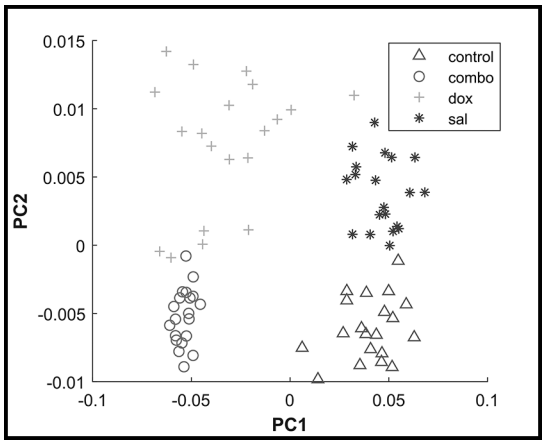

Figure 4: PCA score plot of the IR absorbance spectra from cells with different drug treatments. Data points for cells with the same treatment cluster among themselves, and cells with different drug treatment can be clearly distinguished from each other.

Retinal Implant Project

CNF Project Number: 2504-16

Principal Investigator(s): Douglas Shire, Ph.D.

User(s): Marcus Gingerich, Ph.D.[1,4], Douglas Shire, Ph.D.[1,3,4], Patricia Wong[2,4]

Affiliation(s): 1. Dept. of Electrical Engineering, Cornell University; 2. Dept. of Neuro-Ophthalmology, Massachusetts Eye and Ear Infirmary; 3. VA Cleveland Healthcare System; 4. Bionic Eye Technologies, Inc.

Primary Source(s) of Research Funding: NIH/NIBIB U01EB018873; NIH/NIBIB R01EB022013, Massachusetts Lions Eye Research Fund, DoD W81XWH-16-2-0015

Contact: dbs6@cornell.edu, mdg37@cornell.edu, pwong@bionicvisiontechnologies.com

Website: http://www.bostonretinalimplant.org

Primary CNF Tools Used: PT-72, lithography toolset/MA6, DWL2000, evaporators, AJA sputter, Gamma spray coater, SEMs, gold electro-plating, Class 2 lithography toolset, Oxford PECVD, Oxford 100 etcher, Glenn 1000, YES polyimide oven, VersaLaser

Abstract:

The purpose of the Retinal Implant Project is to restore useful vision to patients who are blind with degenerative retinal diseases. The primary illnesses we hope to treat are retinitis pigmentosa (a primary cause of inherited blindness) and age-related macular degeneration (the leading cause of blindness in the developed world). Both these diseases cause the eventual destruction of the photoreceptor cells — rods and cones — in the retina, leaving intact the ganglion cells that transmit electrical impulses (and hence visual information) to the brain. The ganglion cells may be stimulated, however, with biphasic current pulses from a microfabricated electrode array. Blind surgical volunteers have consistently described visual percepts that resulted from such stimuli, and this has led our team to develop a wireless, implantable retinal prosthesis.

Summary of Research:

The implanted portion of our device consists of power and data secondary receiving coils, and in a sealed titanium (Ti) can a small number of discrete components, and a custom designed application specific integrated circuit (ASIC) that consists of circuitry for clock and data recovery, current drivers for electrodes in a stimulating electrode array, and a programmable function generator capable of stimulating with a wide range of pulse widths and amplitudes. The current outputs drive high-charge capacity sputtered iridium oxide film (SIROF) stimulating electrodes, which in turn give rise to the visual percepts mentioned above.

CNF-fabricated components of this system have included various proof-of-concept test structures and tools used in the research effort and an integrated combination flexible circuit and stimulating electrode array. Si wafers serve as carriers for these freestanding films during processing. The electrode leads are fabricated inside of 'sandwiches' of polyimide and amorphous silicon carbide (SiC), while the SIROF electrodes are reactively sputter-deposited.

Assembly of the intraocular components of the prosthesis is accomplished by flip chip solder ball bonding of the IC and solder attachment of discrete components onto an internal flexible circuit board that is hermetically sealed into an ultraminiature Ti can. The RF coils are soldered and glued to the integrated external flex-array that is in turn thermosonically bonded to the hermetic feedthrough of the Ti can. Finally, the thermosonic bonds are protected and insulated with an over-mold. An external patient interface unit, will consist of a video camera for capturing images, a digital signal processor, and a radio frequency (RF) transmitter and coil to relay power and data to the implanted device.

Scientific challenges still remain in realizing a chronically implantable retinal prosthesis. While our first-generation device was primarily encapsulated in polymers for short term proof-of-concept implant studies, our second-generation system focused on a system that would last many years *in vivo*. Our more recent efforts have focused on developing a device with 256+ stimulation channels,

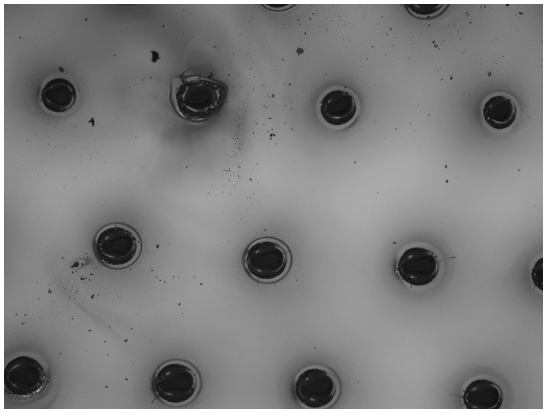

Figure 1: A image of through-wafer holes in a fused silica wafer made with the CNF VersaLaser.

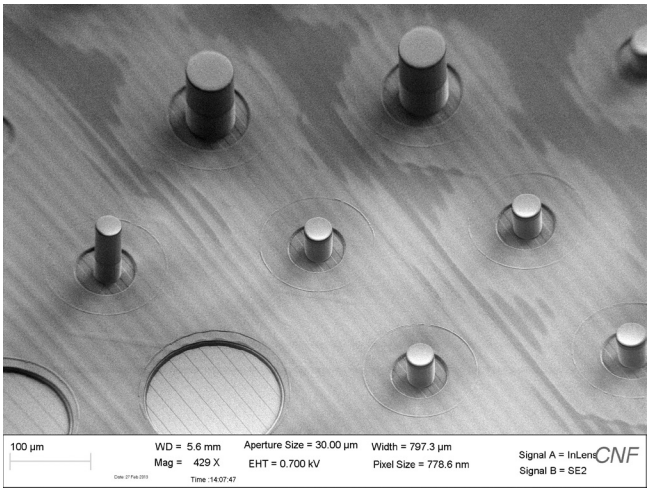

Figure 2: An SEM image of an electrode array of SU-8-based penetrating electrodes and planar electrodes fabricated on the same flexible substrate.

which is still small enough and of a configuration to be easily implanted in the ocular orbit and continue to function for many years *in vivo*. Thus, a major effort has been the development of a technological platform to build a robust, hermetically packaged, high-density subretinal visual prosthesis with a lifetime of > 10 years in biological saline that is scalable to hundreds of I/O channels.

Recent efforts in the CNF have included developing improvements to bonding of electrode arrays to Pt-pin ceramic feedthroughs by electroplating Au onto the surface of the platinum (Pt) pins. This has increased the reliability of the bonds between the electrode array and the ceramic feedthrough. Improvements in assembly techniques, underfilling, overmolding and final parylene-C protection have yielded a passive retinal implant system that has been successfully implanted in an animal model for several months with no significant adverse effects.

Other efforts in the CNF have included developing a fabrication process for indwelling electrodes for long-term implantation in brain tissue. The process currently utilizes low- stress silicon-nitride as the protective layer whereas it is expected that this will transition to silicon-carbide as the material of choice in the future. An economic means of producing a fused-silica feedthrough was also explored utilizing the VersaLaser to create through-wafer holes as shown in Figure 1, but it is not yet clear that this method is capable of producing devices with the necessary hermeticity.

The project has substantially completed the implementation of a microfabrication process to incorporate SU-8-based 3D electrodes into a hybrid electrode array to achieve a more optimal interface between the electrode and the target neural cells. Fabrication work at the CNF has included process development required for such high aspect structures including the challenges of lithography with the presence of extreme topography. Many of these lithographic processes have been successfully realized using the Gamma spray coating tool. Figure 2 shows such an SEM image of an electrode array containing different geometries of SU-8-based penetrating electrodes as well as planar electrodes on the same flexible substrate. The latest microfabrication processes utilize numerous CNF tools including the Heidelberg 2000 mask writer, MA6 aligner, polyimide YES curing oven, PT72 RIE, SC4500 evaporator, Gamma Spray Coater, Au electroplating station, K & S Au ball bonder, Oxford PECVD, Oxford 100 etch tool, Parylene coater, as well as numerous metrology tools.

References:

[1] J. F. Rizzo, J. Wyatt, J. Loewenstein, S. Kelly, and D. Shire, "Methods and Perceptual Thresholds for Short-Term Electrical Stimulation of Human Retina with Microelectrode Arrays," Investigative Ophthalmology and Visual Science, vol. 44, no. 12, Dec. 2003, pp. 5355-5361.

Characterizing the Role of Tumor-Derived Extracellular Vesicles in Breast Cancer

CNF Project Number: 2580-17

Principal Investigator(s): Claudia Fischbach, Lara Estroff

User(s): Aaron Chiou, Rupal Khaitan, Minjee Kang

Affiliation(s): Meinig School of Biomedical Engineering, Cornell University

Primary Source(s) of Research Funding: National Institutes of Health

Contact: cf99@cornell.edu, lae37@cornell.edu, aec267@cornell.edu, rk545@cornell.edu, mk2546@cornell.edu

Website(s): fischbachlab.org, estroff.mse.cornell.edu

Primary CNF Tools Used: Malvern NS300 Nanosight

Abstract:

Breast cancer frequently metastasizes to bone, leading to osteolytic bone degradation and poor clinical prognosis. Therapeutic options are largely ineffective as the mechanisms underlying this process remain unclear. Increasing evidence suggests that primary tumors release soluble factors and extracellular vesicles (EVs) that can systemically prime distant organs for eventual metastasis. We have previously shown that primary breast tumors can alter bone materials properties even prior to secondary tumor formation, suggesting possible interference with bone mineralization pathways [1]. However, it remains unclear whether EVs directly contribute to alterations in the bone microenvironment prior to metastasis, whether their generation depends on tumor malignancy, and whether these vesicles differ in content and function. Our project investigates the connections between EV generation, breast cancer malignancy, the functional effect of EVs on stromal cells present in metastatic sites such as the bone.

Summary of Research:

Tumor-derived EVs, such as microvesicles (0.2-2 μm in size) shed from the plasma membrane and exosomes (30-100 μm) derived from multi-vesicular bodies, are emerging as critical yet distinct mediators of cell-cell communication in cancer. We are exploring the role of EVs in breast cancer metastasis to bone by isolating EVs from a panel of breast cancer cell lines representing varying degrees of malignancy to 1) characterize the amount and size distribution of EVs generated, and 2) evaluate their interaction with bone-mimetic microenvironments, and 3) evaluate their effects on stromal cells present in the bone microenvironment. By studying these phenomena, we hope to identify novel insights on bone metastasis progression that may inform the development of more effective treatments.

To investigate these questions, we have begun by culturing breast cancer cell lines of varying malignant potential and collecting the EVs shed by these cell lines. We are using the Nanosight instrument to analyze the size distributions and measure concentrations of EVs shed by these cell lines.

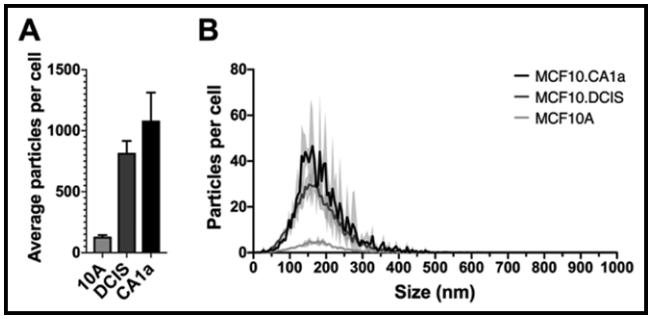

Figure 1: EV concentration and size distributions as measured by Nanosight. (a) Average number of EVs shed per cell increases with breast cancer cell malignancy potential (in increasing order: MCF10A, MCF10. DCIS, MCF10.CA1a). (b) Histograms of EV size distribution indicate increasing amounts of both microvesicles and exosomes shed by cells of increasing malignancy potential.

Our findings in Figure 1 indicate that compared to their benign counterparts, cell lines that represent more invasive and metastatic potential shed a greater amount of EVs per cell, with increases in both microvesicles and exosomes.

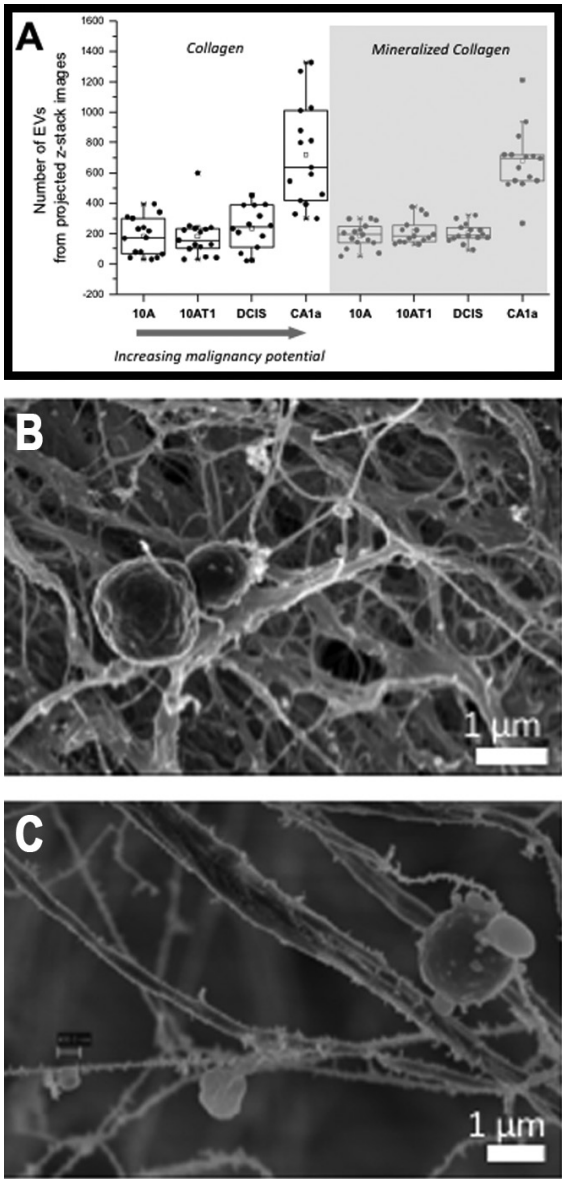

Figure 2: EVs within non-mineralized and mineralized collagen scaffolds analyzed via confocal imaging and SEM. (a) EVs shed from more malignant breast cancer cells (MCF10CA1a) show better binding ability than those shed from less malignant cells both in microenvironments. (b,c) Representative SEM images of MCF10CA1a cell-shed EVs bound to (b) collagen fibrils and (c) mineralized collagen fibrils.

Next, we have also labelled these EV populations and incubated them into collagen scaffolds with and without mineralization to examine their interactions with bone-mimetic microenvironments. As shown in Figure 2, we have imaged these EVs via confocal microscopy and found that the number of EVs bound to these bone-mimetic matrices was 3-8 fold greater when derived from more malignant cells compared to less malignant cells. Using scanning electron microscopy (SEM), we can visualize EVs from malignant cells bound to the non-mineralized and mineralized collagen fibrils in the bone-mimetic microenvironments.

These findings suggest that tumor-shed EVs, in particular those from more malignant tumor cells, can effectively bind to components of the bone microenvironment, and thus may play a role in priming the bone for subsequent metastasis. We are pursuing further investigation of the mechanisms by which these EVs bind to the bone microenvironment, as well as the effects of these EVs on bone-resident stromal cells and tumor cells within bone-mimetic microenvironments.

References:

[1] He F, Chiou AE, Loh HC, Lynch ME, Seo BR, Song YH, Lee MJ, Hoerth R, Bortel E, Willie B, Duda G, Estroff LA, Masic A, Wagermaier W, Fratzl P, Fischbach C. Multiscale characterization of the mineral phase at skeletal sites of breast cancer metastasis. Proceedings of the National Academy of Sciences, 114(40), 10542-10547. https://doi.org/10.1073/pnas.1708161114 (2017).

Circulating Extracellular Vesicles and Physical Stress in ME/CF

CNF Project Number: 2590-17
Principal Investigator(s): Maureen R. Hanson
User(s): Adam O'Neal, Ludovic Giloteaux

Affiliation(s): Department of Molecular Biology and Genetics, Cornell University, Ithaca, NY 14853
Primary Source(s) of Research Funding: National Institutes of Health
Contact: mrh5@cornell.edu, ajo39@cornell.edu, lg349@cornell.edu
Website: https://neuroimmune.cornell.edu/research/vesicles-and-signaling/
Primary CNF Tools Used: Malvern NS300 Nanosight

Abstract:

Myalgic Encephalomyelitis/Chronic Fatigue Syndrome (ME/CFS) is a chronic, complex, multisystemic condition characterized by long-term fatigue that does not improve with rest, persists for more than six months, and other associated symptoms, and cannot be explained by any other underlying medical condition. The cause of ME/CFS remains unknown, and no established diagnostic tests, nor universally effective treatment are available.

Introduction:

A hallmark of ME/CFS is a distinctive Post-Exertional Malaise (PEM), which occurs following physical or cognitive exertion and can last from days to weeks. Research on the physiological responses to exercise in ME/CFS subjects supports disruptions and disturbances in the central nervous system, cardiovascular and immune system with impaired muscular energy metabolism. Following exercise challenge, skeletal muscle can impact the whole body physiology through secretion of diverse biomolecules into exosomes (exersomes) such as muscle-derived humoral factors (myokines) and exercise-induced humoral factors (exerkines) in a regulated and targeted manner.

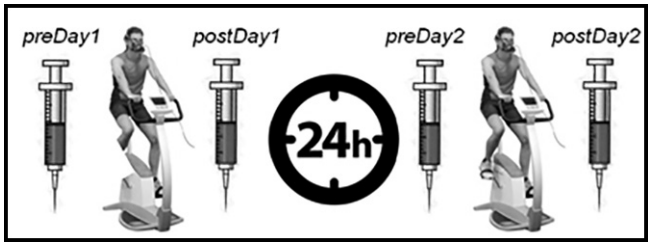

Figure 1: ME/CFS patients and age-and gender-matched sedentary controls will perform two successive CPETs, separated by 24 hours. EVs will be characterized in blood samples taken at four different time points, preDay1, postDay1, preDay2, and postDay2.

Extracellular vesicles (EVs), once ignored, are now receiving increasing attention as various roles in signaling in cancer, nervous system disorders, innate immunity, pregnancy, and stress responses have become evident [1,2]. Several types of extracellular vesicles have been described, as well as identifying markers [1]. Exosomes, a specific type of EV, are small membrane-bound vesicles that are 30-120 nm in diameter that are released into the extracellular environment by various cell types when internal bodies fuse with the plasma membrane. Exosomes contain cargo such as proteins, lipids, hormones, and RNAs (especially miRNAs) that can influence the function of the cells with which they fuse. One possibility is that exosomes and other types of EVs are involved in cell-to-cell signaling that results in abnormalities in ME/CFS patients' immune function and metabolism at baseline but particularly after any exertion (see Figure 1). In healthy individuals, exercise is known to result in the release of exosomes [3], but there are no published studies on the effect of exercise on EVs in ME/CFS. The size distribution and concentration of isolated exosomes/EVs will be performed using Nanoparticle Tracking Analysis on the Malvern NS300 Nanosight instrument.

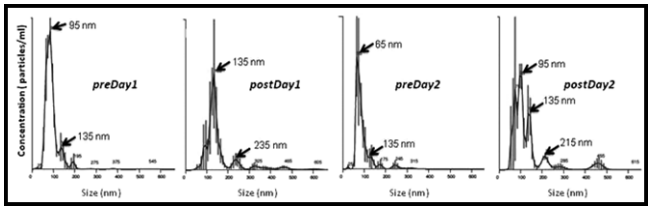

Figure 2: Changes in EV size distribution before and after two exercise challenges on consecutive days, as measured by Nanoparticle Tracking Analysis.

Summary of Research:

We examined EV size and concentration in plasma from 35 ME/CFS patients and 35 healthy controls. By performing NTA with the Malvern NS300 Nanosight, we found that the concentration of the exosome size class was increased in the patient plasma, though the concentration of the total EV population was not significantly different. The aforementioned plasma was collected the same day as the blood draw. We used a second population in which blood was shipped overnight before plasma was collected.

In this second population, we observed that the concentration of all size classes of EVs and the average size of the EVs were significantly increased in the patient plasma. A pilot experiment with blood taken at four time points in shown in Figure 2 and demonstrates the expected increase in size and concentration after exercise.

References:

[1] Yanez-Mo M, Siljander PR, Andreu Z, Zavec AB, Borras FE, Buzas EI, Buzas K, Casal E, Cappello F, Carvalho J, Colas E, Cordeiro-da Silva A, Fais S, Falcon-Perez JM, Ghobrial IM, Giebel B, Gimona M, Graner M, Gursel I, Gursel M, Heegaard NH, Hendrix A, Kierulf P, Kokubun K, Kosanovic M, Kralj-Iglic V, Kramer-Albers EM, Laitinen S, Lasser C, Lener T, Ligeti E, Line A, Lipps G, Llorente A, Lotvall J, Mancek-Keber M, Marcilla A, Mittelbrunn M, Nazarenko I, Nolte-'t Hoen EN, Nyman TA, O'Driscoll L, Olivan M, Oliveira C, Pallinger E, Del Portillo HA, Reventos J, Rigau M, Rohde E, Sammar M, Sanchez-Madrid F, Santarem N, Schallmoser K, Ostenfeld MS, Stoorvogel W, Stukelj R, Van der Grein SG, Vasconcelos MH, Wauben MH, De Wever O (2015) Biological properties of extracellular vesicles and their physiological functions. J Extracell Vesicles 4: 27066.

[2] Desrochers LM, Antonyak MA, Cerione RA (2016) Extracellular Vesicles: Satellites of Information Transfer in Cancer and Stem Cell Biology. Dev Cell 37: 301-309.

[3] Safdar A, Saleem A, Tarnopolsky MA (2016) The potential of endurance exercise-derived exosomes to treat metabolic diseases. Nat Rev Endocrinol 12: 504-517.

Development of Microfluidic Device for Protein Synthesis and Modification

CNF Project Number: 2641-18

Principal Investigator(s): Susan Daniel

User(s): Zachary Manzer

Affiliation(s): Smith School of Chemical and Biomolecular Engineering, Cornell University

Primary Source(s) of Research Funding: National Science Foundation

Contact: sd386@cornell.edu, zam42@cornell.edu

Primary CNF Tools Used: Heidelberg DWL66fs mask writer, ABM contact aligner, Unaxis 770 deep Si etcher, Anatech resist strip, MVD 100, P10 profilometer, FilMetrics F50-EXR

Abstract:

Current biological production limits our ability to produce and study tailored biological therapeutics. Many important targets need post-translational modifications that are necessary for maintaining proper structure and function [1]. The cell naturally uses membrane-bound enzymes to do this in a regulated and compartmentalized way. We aim to create a microfluidic device that can recreate this cellular assembly line an in a synthetic system while still maintaining the natural biological environment. The first step in this process is the protein synthesis, which we have shown in this work. Since the flow characteristics, channel dimensions, and the local environment are readily controlled, this platform gives us a way to easily mimic and manipulate the local environment to efficiently produce a protein of interest. Future work will focus on the incorporation of the enzymes into a supported membrane in the device.

Summary of Research:

Previous work in cell-free protein synthesis has been done in static reaction conditions [2]. We aim to build on this body of work and build a platform with continuous flow protein synthesis in conjunction with the selective patterning of necessary enzymes to modify them in a precise way. To design the microfluidic device, first a negative mask for a prototype microfluidic design was created using the Heidelberg DWL66fs mask writer and used with the ABM contact aligner to pattern photoresist that was spun onto a silicon wafer. After development, the profile of the patterns was analyzed on the P10 profilometer. Optimization of the process was conducted to produce consistent and even films, as measured by the profilometer and the FilMetrics F50-EXR. Once this was done, the exposed silicon was etched using the Unaxis 770 deep Si etcher. Photoresist on the channels was removed by oxygen plasma cleaning in the Anatech resist strip. A final hydrophobic coating (FOTS) was applied using molecular vapor deposition to allow for PDMS molds to be easily removed once cast.

Once the mold was fabricated, Sylgard 184 was poured over the mold and cured. This could then be removed and bonded to a glass coverslip by using oxygen plasma cleaning on both surfaces.

The first step in creating this device is the successful synthesis of a model protein. By collecting the cellular machinery, proteins can be produced in an *in vitro* environment [3]. We isolate a plasmid encoding the green fluorescent protein (GFP) and a cell lysate, and by mixing them together, we produce GFP.

As seen in Figure 1, we can inject each of them independently and through the mixing in the channels, GFP is produced as they proceed through the channels. The small volume of the microfluidic gives tighter temperature control by limiting heat transfer and enhances diffusion to give a higher rate of synthesis as compared to the test tube.

Future work will involve the synthesis of more relevant protein targets as well as the incorporation of enzymes into the supported membrane for modification of the proteins produced.

References:

[1] Defaus, S., Gupta, P., Andreu, D., and Gutiérrez-Gallego, R. Mammalian protein glycosylation - structure versus function. Analyst 139, 2944-2967 (2014).

[2] Swartz, J. R. Advances in Escherichia coli production of therapeutic proteins. Curr. Opin. Biotechnol. 12, 195-201 (2001).

[3] Mohr, B. P., Retterer, S. T., and Doktycz, M. J. While-you-wait proteins? Producing biomolecules at the point of need. Expert Rev. Proteomics 13, 707-709 (2016).

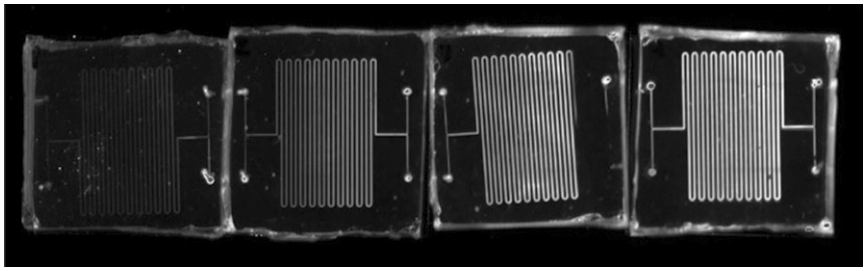

Figure 1: Series of microfluidic devices that were used to produce GFP in a cell-free continuous flow reaction. DNA and cell lysate are introduced independently on the left side and mix as they enter the first device. The increase in fluorescence across the image is seen as the protein increases in concentration through the length of the channels.

Development of a Heparin-Based Coacervate Loaded Liposomes as Non-Invasive Therapy for Myocardial Infarction

CNF Project Number: 2754-18

Principal Investigator(s): Yadong Wang

User(s): Chia-Wei Yeh

Affiliation(s): Biomedical Engineering, Cornell University

Primary Source(s) of Research Funding: Cornell Startup Funds

Contact: yw839@cornell.edu, cy465@cornell.edu

Primary CNF Tools Used: ABM contact aligner

Abstract:

Cardiovascular disease is one of the major leading causes of death worldwide. Specifically, myocardial infarction (MI), generally known as heart attack, is the main cause of death in cardiovascular disease. Among them, the major cause of death of MI is due to the myocyte necrosis and heart failure. Therefore, it is of particular importance to prevent myocyte necrosis after MI as well as induce infarcted heart tissue to regenerate.

Introduction:

Coacervate is an electrostatically bound complex between cationic and anionic polyelectrolytes. In the extracellular matrix (ECM), glycosaminoglycan such as heparan sulfate proteoglycan (HSPG) binds with several growth factors (GFs) to form HSPG-GF complex. This complex not only serves as reservoir for bonding and stabilization of GFs but also potentiates GFs responsible for maintaining normal cellular function. Due to the similar mechanism of protein-extracellular matrix interaction, it has been shown that heparin-based coacervate is a promising candidate for drug delivery system in biomedical and tissue engineering applications. However, coacervate complex is unstable in the blood stream owing to the relatively weak electrostatic interaction within coacervate droplets, leading to the difficulty to systemically administer coacervate via intravenous injection.

To solve this problem, we aim to encapsulate heparin-based coacervate complex into liposome, namely coacersome, for a non-invasive therapy for MI. In this study, polyanion heparin is utilized to complex with vascular endothelial growth factors C (VEGF-C) to form heparin-growth factor complex, which is then mixed with synthetic polycation, ploy(ethylene arginyl aspartate diglyceride) (PEAD) to construct VEGF-C loaded coacervate droplets. In order to enhance coacervate complex stability in the blood stream, an on-chip microfluidic device is used to generate coacersomes by encapsulating VEGF-C loaded coacervates into liposomes in a well-defined manner. The therapeutic effect of the coacersomes will be evaluated on rat myocardial infarction model.

Summary of Research:

The microfluidic device is designed to generate liposomes encapsulated with coacervate complex in different size by using different flow rate among outer aqueous phase (OA), inner aqueous phase (IA), and lipid carried organic phase (LO), as shown in Figure 1. OA contains 15% (vol/vol) glycerol and 5% (w/v) P188 in water, IA contains 15% (vol/vol) glycerol and 20 μg/mL FITC-heparin water, and LO contains 0.2% (wt/vol) DOPC in 1-octanol. Liposomes are successfully generated via microfluidic device, and the flow rate is 5 μL/min for each phase, as shown in Figure 2. At this time point, the size distribution is wide — the diameter of liposome ranges from 10 to 200 μm.

Next, FITC-heparin is successfully encapsulated into DOPC liposomes, and the flow rate is 0.1 μL/min for each phase, as shown in Figure 3. The diameter of FITC-heparin encapsulated DOPC liposome ranges from few microns to 10 μm. The encapsulation efficiency is 40% to 50% at this time point. In order to generate liposomes in different size, two different flow rate are used to generate DOPC liposomes (0.1 μL/min and 5 μL/min for each phase, as shown in Figure 4), and the diameter is different. However, detailed size distribution is not tested at this time point.

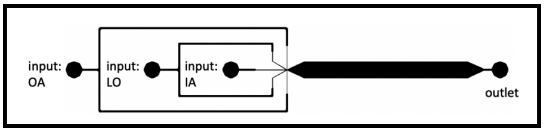

Figure 1: Water-in-oil-in-water double emulsion chip for generating liposome encapsulated with coacervate. OA: outer aqueous phase; IA: inner aqueous phase; LO: lipid carried organic phase.

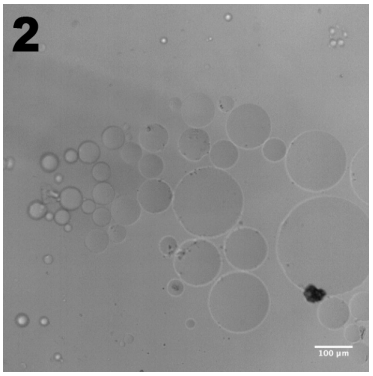

Figure 2: DOPC liposomes generated via microfluidic device. Scale bar: 100 µm.

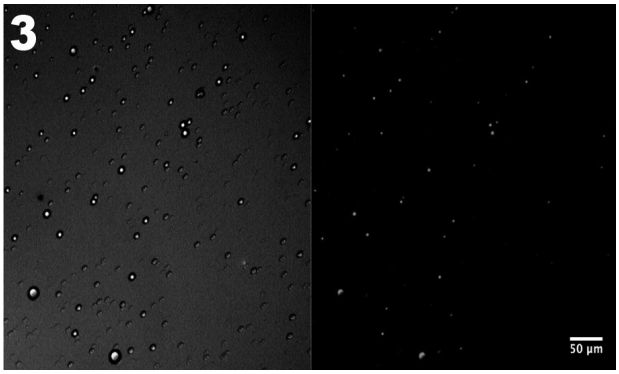

Figure 3: FITC-heparin encapsulated DOPC liposomes, gray scale and fluorescent images. Scale bar: 50 µm.

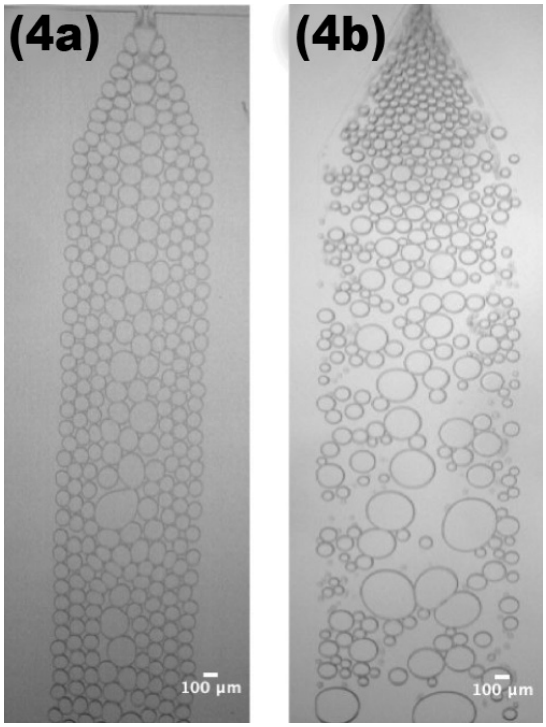

Figure 4: DOPC liposomes generated via microfluidic device. (a) flow rate: 0.1 µL/min for each phase. (b) flow rate: 5 µL/min for each phase. Scale bar: 100 µm.

References:

[1] Deshpande, Siddharth, and Cees Dekker. "On-chip microfluidic production of cell-sized liposomes." Nature protocols 13.5 (2018): 856.

[2] Deshpande, Siddharth, et al. "Spatiotemporal control of coacervate formation within liposomes." Nature communications 10.1 (2019): 1800.

Phytophthora Zoospore Chemotaxis

CNF Project Number: 2774-19
Principal Investigator(s): Denis S. Willett
User(s): Bo Holladay

Affiliation(s): Department of Entomology, Cornell AgriTech (New York State Agricultural Experiment Station)
Primary Source(s) of Research Funding: Cornell University Start-Up
Contact: deniswillett@cornell.edu, bh542@cornell.edu
Primary CNF Tools Used: Photolithography, mask writing, spinner

Abstract:

***Phytophthora* oomycetes (greek for 'plant destroyer') cause devastating losses to many food crops and are responsible for the Irish potato famine in the 1800s. Phytophthora can attack plants with single-celled zoospores. These zoospores respond to chemical cues released by plants to decide where to attack. This project evaluates zoospore response to chemical cues to prevent *Phytophthora* infection.**

Summary of Research:

Phytophthora is perhaps the most devastating plant pathogen affecting the human food system and is a major pathogen affecting vegetable production (squash, pumpkin, cucumber, pepper, eggplant, tomato, and snap beans) in NY State. *Phytophthora capsici* is now established in 25 NY counties and has been detected in 100% of irrigation sources in two regions of the state. Management currently relies on intensive fungicide regimes, but left unmanaged, *Phytophthora* losses can reach 100%. *Phytophthora* infection spreads through travel of single-celled swimming zoospores, which use flagella to propel themselves through aqueous media. These zoospores can travel relatively long distances under their own power and respond to chemical cues in their environment. These cues include volatiles released by plants; *Phytophthora* zoospores can be repelled or attracted by these cues and can choose to move toward or away from them. Using a combination of single-cell microfluidic chip bioassays, analytical chemistry techniques, microcosm bioassays, and field experiments we seek to evaluate chemical cues for controlling and preventing *Phytophthora* zoopsore infection.

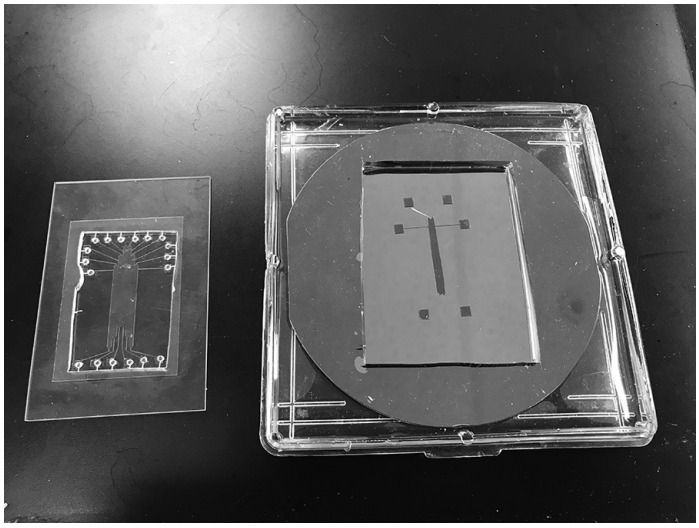

Figure 1: Microfluidic chips made to study Phytophthora *zoospore chemotaxis.*

Previous work has determined zoospore motile ability and suggested specific plant volatiles as potential attractants and repellents. This work will focus on evaluating these cues for applications to New York vegetable crops. These chemical ecology based techniques will provide producers with a potent tool for managing devastating *Phytophthora* infection in the high-value vegetable crops of New York State.

Characterization of Cancer Microvesicles

CNF Project Number: 2780-19

Principal Investigator(s): Cynthia Leifer, Tracy Stokol

User(s): Christopher Wan, Jingyi Chen

Affiliation(s): Microbiology and Immunology, and Population Medicine and Diagnostic Sciences, College of Veterinary Medicine, Cornell University

Primary Source(s) of Research Funding: Physical Sciences Oncology Center Pilot Project

Contact: cynthia.leifer@cornell.edu, ts23@cornell.edu, cw685@cornell.edu, jc2876@cornell.edu

Website: https://www.leiferlab.com/

Primary CNF Tools Used: Malvern NS300 Nanosight

Abstract:

Pathologic activation of hemostasis in cancer is associated with systemic thrombotic events and transformation, growth and metastasis of various tumors [1,2]. Tissue factor (TF), the main activator of coagulation, is over-expressed in breast tumors *in situ* and in breast cancer cell lines, particularly triple negative cells [3,4] and expression in patient tumors is correlated with a poor prognosis [3]. Cancer-associated TF produces coagulation factor complexes that trigger thrombosis and induce cell signaling via protease-activated receptors (PARs). Macrophages are recruited from bone marrow-derived cells and blood monocytes and play key roles in pathologic hemostasis. Exposure to cancer cells and the tumor microenvironment induces a protumorigenic, pro-angiogenic, and immunosuppressive phenotype in tumor-associated macrophages [9]. However, it is unknown whether breast cancer cell-generated TF-coagulation complexes and PARs regulate macrophage recruitment to tumors or whether they subsequently modulate macrophage behavior in tumors. This is important since macrophage recruitment and regulation contributes to angiogenesis, metastasis and tumor progression [10-12].

Introduction:

We hypothesize that breast cancer-associated hemostatic components regulate macrophage recruitment and their inflammatory, angiogenic and hemostatic activity. To investigate this question, we have demonstrated that conditioned media from a mouse breast cancer cell line enhances procoagulant activity of mouse macrophages. To determine the active component of the conditioned media, we isolated the microvesicles by ultracentrifugation and showed they had intrinsic procoagulant activity and conferred procoagulant activity to macrophages. We used the Nanosight NS300 to characterize the microvesicle populations purified from cancer cell-conditioned and control media.

Data obtained using the Nanosight NS300 confirmed that we isolated particles < 100 nm, compatible with exosomes. Altogether, our data show that breast cancer-derived microparticles confer procoagulant activity to macrophages, which may play a key role in the connection between coagulation and inflammation to regulate tumor growth and anti-tumor immunity.

Summary of Research:

In this project, we tested the procoagulant activity of a mouse breast cancer cell line and found that the cells accelerated clotting in mouse plasma. We isolated the microvesicle fraction shed from the mouse breast cancer cell line into conditioned media using ultracentrifugation and tested the procoagulant activity of the isolated microvesicle fraction. We found that the microvesicle fraction also demonstrated procoagulant activity. Overnight incubation of a mouse macrophage cell line with the isolated microvesicle fraction from tumor-conditioned, but not cell-free, media increased the procoagulant activity of the mouse macrophage cell line. This supports our hypothesis that tumor cells upregulate procoagulant activity in macrophages. Our goal with using the Cornell NanoScale Facility was to characterize the size distribution of the obtained microparticles, using cell-free media as a negative control. For this we used the Nanosight NS300 instrument. We found that the microvesicle fraction consisted of a dominant population of particles < 100 nm, supporting successful isolation of exosomes shed from tumor cells (Figure 1).

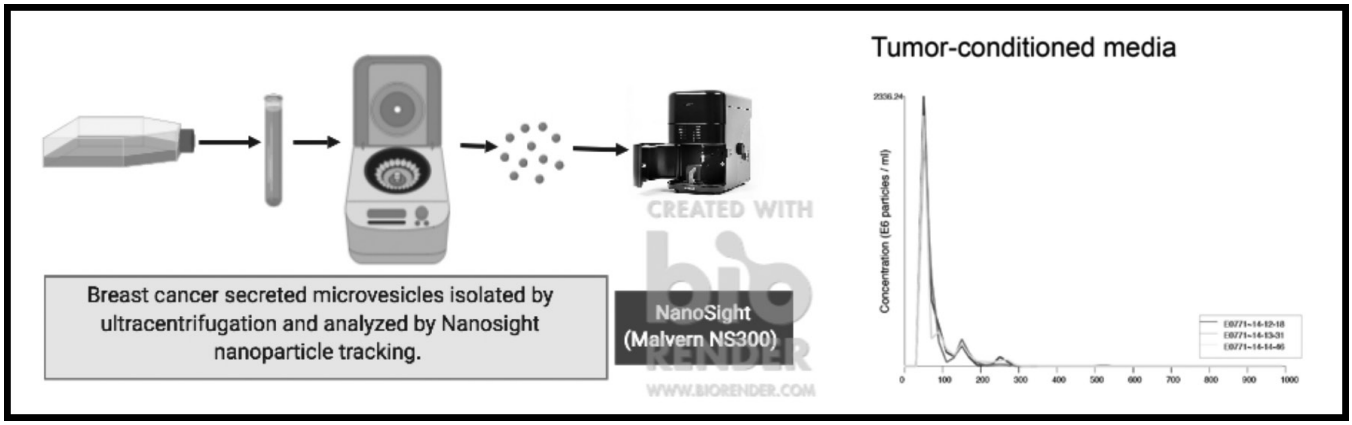

Figure 1: Schematic for nanoparticle isolation and analysis using the Nanosight. Example results of nanoparticle tracking analysis of microvesicles isolated by ultracentifugation from mouse breast cancer cell tumor-conditioned media. A high concentration of particles < 100 nm, compatible with exosomes, was found in the tumor-conditioned media preparation.

References:

[1] Khan UT, Walker AJ, Baig S, et al. Venous thromboembolism and mortality in breast cancer: cohort study with systematic review and meta-analysis. BMC Cancer 2017;17:747.

[2] Cole M, Bromberg M. Tissue factor as a novel target for treatment of breast cancer. Oncologist 2013;18:14-18.

[3] Vrana JA, Stang MT, Grande JP, et al. Expression of tissue factor in tumor stroma correlates with progression to invasive human breast cancer: paracrine regulation by carcinoma cell-derived members of the transforming growth factor beta family. Cancer Res 1996;56:5063-70.

[4] Che SPY, Park JY, Stokol T. Tissue Factor-Expressing Tumor-Derived Extracellular Vesicles Activate Quiescent Endothelial Cells via Protease-Activated Receptor-1. Front Oncol 2017;7:261.

[5] Versteeg HH, Schaffner F, Kerver M, et al. Inhibition of tissue factor signaling suppresses tumor growth. Blood 2008;111:190-9.

[6] Bourcy M, Suarez-Carmona M, Lambert J, et al. Tissue Factor Induced by Epithelial-Mesenchymal Transition Triggers a Procoagulant State That Drives Metastasis of Circulating Tumor Cells. Cancer Res 2016;76:4270-4282.

[7] Palumbo JS, Talmage KE, Massari JV, et al. Tumor cell-associated tissue factor and circulating hemostatic factors cooperate to increase metastatic potential through natural killer cell-dependent and -independent mechanisms. Blood 2007;110:133-141.

[8] Eftekhari R, de Lima SG, Liu Y, et al. Microenvironment proteinases, proteinase-activated receptor regulation, cancer and inflammation. Biol Chem 2018;399:1023-1039.

[9] Aras S, Zaidi MR. TAMeless traitors: macrophages in cancer progression and metastasis. Br J Cancer 2017;117:1583-1591.

[10] Gil-Bernabé AM, Ferjancic S, Tlalka M, et al. Recruitment of monocytes/macrophages by tissue factor-mediated coagulation is essential for metastatic cell survival and premetastatic niche establishment in mice. Blood 2012;119:3164-3175.

[11] Lin L, Chen Y-S, Yao Y-D, et al. CCL18 from tumor-associated macrophages promotes angiogenesis in breast cancer. Oncotarget 2015;6:34758-34773.

[12] Su S, Liu Q, Chen J, et al. A positive feedback loop between mesenchymal-like cancer cells and macrophages is essential to breast cancer metastasis. Cancer Cell 2014;25:605-620.